

**Co-Editor Decision: Reconsider after minor revisions (Editor review) (03 Apr 2017)** by James Allan

Comments to the Author:

While the paper looks good on the whole, there were certain 'major' comments from both referees that I do not see as being adequately addressed. I would like to see these tackled properly before the paper goes to publication.

Firstly, regarding referee #1's comment concerning anthropogenic influence, I note that the authors have rebutted this point, however I see that as a sufficiently important issue that this should be addressed in the manuscript itself. I would ask that the authors amend the text to reflect this.

*In the summary and conclusions we added the text:*

*In this analysis the possibility that sporadic anthropogenic emissions were interpreted as NPF events cannot be excluded completely. However, there are a number of facts arguing strongly against this possibility leading to serious misinterpretation of the data:*

- a) *Location and operation of the Mt. Zeppelin station exclude local contamination to a very large extent.*
- b) *Manual inspection of the time series by one of the co-authors (PT) further reduced the risk of contaminated data.*
- c) *The temporal evolution of MEV events, i.e. concurrent and sustained concentration increases at several particle sizes below 60 nm does not correspond to a typical passage of stack emissions from a large combustion source, (Ogren and Heintzenberg, 1990). Instead, it looks very much like MEV events observed under even stricter constraints on local or regional sources of contamination on icebreaker Oden in the central pack ice area, (Karl et al., 2013), and also looks similar to nocturnal NPF-events in Australian forests, (Suni et al., 2008; Junninen et al., 2008).*

Second, referee #2's points 1 and 2 about the metrics being reported has not been addressed, which they regard as being very important (see their comments). However, on reading the rebuttal and the paper referenced by the referee, it seems to me that the authors may have misunderstood what the referee was asking for. The metrics in question are defined in the paper Kulmala et al. (2012) doi:10.1038/nprot.2012.091, where 'GR' is defined as 'growth rate' and 'CS' as 'condensation sink'. Furthermore, the term 'formation rate' is applied to the rate of particle number formation at a defined size, not the growth rate referred to in section 3.2 and in the rebuttal.

In light of this clarification, can the authors generate these metrics and comparisons, as requested? I would expect that this would be most appropriate as an extension to the DGR approach. As well as ensuring comparability with other works, this will also allow the dataset to be more accessible for any future meta-analyses. Even if these comparisons turn up null results, this would still be an important observation to report in its own right. If the authors still feel that generating these statistics would be inappropriate, they are still entitled to make that argument, but such an argument should probably be reflected in the text of the paper, so as not to leave it open to accusations of deliberate omission. I should state however that my personal inclination is to err on the side of generating these statistics unless there is a technical reason that prevents this.

*In response we modified the discussion of DGR-events and added the following text and Table 3:*

*In the analysis of atmospheric data and theoretical modeling of NPF-events of type DGR two key parameters are discussed, namely particle formation rate  $J$  ( $\text{cm}^{-3}\text{s}^{-1}$ ) and growth rate  $GR$  ( $\text{nmh}^{-1}$ ) of particle diameters. For both parameters the measurement protocol by*

Kulmala et al. (2012) provides specific calculation procedures, (equations. 2, 7, and 9), which we follow in the present study, albeit with the caveat that the one-hour temporal resolution of our time series is far below the ten-minute time resolution that the protocol of Kulmala et al. (2012) requests in order to be able to follow the rapid development of NPF-events. Furthermore, only the 127 DGR-events identified from 2011 on are based on particle size distributions measured down to a diameter of five nanometers.

The sizes of newly nucleated aerosol particles are of order 1–2 nm, which is below or near the limit of existing measurement techniques. When the nuclei grow in size their number concentration decreases because of various removal mechanisms. Instead of particle formation rates at the initial nucleus size so-called apparent nucleation rates  $J_x$  are often reported, i.e. rates at which new particles appear at some larger observable particle diameter  $dx$ . For the present study two apparent nucleation rates are calculated: DGR events of the whole time series have been identified with particle size distributions measured at diameters from 10 nm up through the growth of the number median diameter  $D_{50}$  in the size range 10 – 50 nm. Thus we calculated  $J_{22}$  for these 235 events at the nominal geometric mean diameter of 22 nm. For 127 of these events size distributions reached down to five nanometer diameter, (years 2011 and later). For these events we calculated  $J_{11}$  at the geometric mean diameter 11 nm as representative for the diameter range 5 – 25 nm, which is close to the frequently reported apparent formation rate  $J_{10}$  at 10 nm diameter. Additionally, the two corresponding grow rates  $GR_{22}$  and  $GR_{11}$  were calculated in the respective diameter ranges.

Statistics of these four key parameters of the DGR events are collected in Table 3.

Depending on the pollution level at the measuring site widely varying values of  $J_{10}$  have been reported. For the polluted subtropical environment of Taiwan Young et al. (2013) give values from 4.4 to 30  $\text{cm}^{-3}\text{s}^{-1}$  whereas Pierce et al. (2014) published values between 0.22 and 0.84  $\text{cm}^{-3}\text{s}^{-1}$  from a rural Canadian setting. The latter range is within the range 0.1 – 9.4  $\text{cm}^{-3}\text{s}^{-1}$  with a median value of 1.2  $\text{cm}^{-3}\text{s}^{-1}$  reported by Yli-Juuti et al. (2009) for a station in rural Hungary. The two formation rates of the present study cover the range 0.1 – 1.4  $\text{cm}^{-3}\text{s}^{-1}$  for the 25% to 75% percentiles (see Table 3), which covers the range of 0.05 to 0.13  $\text{cm}^{-3}\text{s}^{-1}$  given by Vencaz et al. (2009) for a remote site in the Himalaya. The environmental conditions at the Siberian station Tiksi at the coast of the Laptev Sea may come closest to our Arctic setting. From this site Asmi et al. (2016) published formation rates of 0.01 to 0.41 at an unspecified particle size.

In terms of 25% to 75% percentiles the particle growth rates of the present study range from 0.4 to 1.4  $\text{nmh}^{-1}$  in the range 5 – 25 nm and 1.0 to 1.8  $\text{nmh}^{-1}$  in the diameter range 10 - 50 nm, which is near the range of results of 1 – 2  $\text{nmh}^{-1}$  derived by Ström et al. (2009) for new particle formation in the lower boundary over Ny-Ålesund, Spitsbergen but considerably lower than the maximum growth rate of 3.6  $\text{nmh}^{-1}$  reported by Asmi et al. (2016) for July at the Siberian station Tiksi at the coast of the Laptev Sea. For open ocean new particle formation events over the North Atlantic O’Dowd et al. (2010) report a “typical growth rate” of 0.8  $\text{nmh}^{-1}$ , whereas Ehn et al. (2010) give an average growth rate of 3  $\text{nmh}^{-1}$ . We note that the average length of DGR-events was  $10 \pm 1$  h, (one standard deviation).

| <b>Statistics</b> | <b>J11</b> | <b>GR11</b> | <b>J22</b> | <b>GR22</b> |
|-------------------|------------|-------------|------------|-------------|
| Minimum           | 0.1        | -1.2        | 0.1        | -0.1        |
| 25%               | 0.4        | 0.1         | 0.2        | 1.0         |
| 50%               | 0.7        | 0.4         | 0.3        | 1.4         |

|         |     |     |     |     |
|---------|-----|-----|-----|-----|
| 75%     | 1.4 | 0.6 | 0.7 | 1.8 |
| Maximum | 19  | 2.2 | 22  | 4   |

*Table 3 Statistics of particle formation rates of DGR-events J11, and J22, ( $\text{cm}^{-3}\text{s}^{-1}$ ), at the nominal geometric mean diameters 11 nm, and 22 nm and corresponding diameter growth rates GR11, and GR22, ( $\text{nmh}^{-1}$ ) in the two diameter ranges 5 – 25 nm, and 10 – 50 nm.*

Finally, I think the point referee #2 had in their point 3 was not how the PCT events had been defined, but that there was no comparison with similar results in the literature. I think whether these the observations defined this way definitely represent NPF is likely to be a moot point, however a paper of this nature should be placed in the context of other works where possible. A quick comparison with other works would be welcome.

*We are afraid to admit that we cannot find any reports in the literature that could be used in comparison to our findings concerning PCT-events. Any suggestions by the reviewer would have been highly welcome.*

As a separate issue concerning referee #1's point regarding trajectory accuracy, I do not regard the issue of back trajectory validation to be one that is easily solved. Because the arctic region is so data-poor, it is highly likely that the wind field used has assimilated (and placed great weighting on) local weather observations. As a result, good agreement here is not surprising but does not necessarily validate the fidelity of the model field away from the observations. I think it should be sufficient to state that there are inherent uncertainties with this technique.

*In the first revision of the manuscript we did address referee #1's point regarding trajectory accuracy by adding "Trajectories extending backwards for ten days are inaccurate at origin due to the trajectory uncertainty of 25-30% of its length, (Stohl, 1998)". Please let us know if you want us to elaborate the point of trajectory accuracy any further.*

Non-public comments to the Author:

And yes, I do think the referee could have been clearer about what they were asking for.

Apologies for the delays in the review process; this is due to factors outside of my control.

## Literature

- Asmi, E., Kondratyev, V., Brus, D., Laurila, T., Lihavainen, H., Backman, J., Vakkari, V., Aurela, M., Hatakka, J., Viisanen, Y., Uttal, T., Ivakhov, V., and Makshtas, A.: Aerosol size distribution seasonal characteristics measured in Tiksi, Russian Arctic, *Atmos. Chem. Phys.*, 16, 1271-1287, 10.5194/acp-16-1271-2016, 2016.
- Ehn, M., Vuollekoski, H., Petäjä, T., Kerminen, V.-M., Vana, M., Aalto, P., de Leeuw, G., Ceburnis, D., Dupuy, R., O'Dowd, C. D., and Kulmala, M.: Growth rates during

- coastal and marine new particle formation in western Ireland, *J. Geophys. Res.*, 115, n/a-n/a, 10.1029/2010JD014292, 2010.
- Kulmala, M., Petäjä, T., Nieminen, T., Sipilä, M., Manninen, H. E., Lehtipalo, K., Dal Maso, M., Aalto, P. P., Junninen, H., Paasonen, P., Riipinen, I., Lehtinen, K. E. J., Laaksonen, A., and Kerminen, V.-M.: Measurement of the nucleation of atmospheric aerosol particles, *Nat. Protocols*, 7, 1651-1667, <http://www.nature.com/nprot/journal/v7/n9/abs/nprot.2012.091.html> - supplementary-information, 2012.
- O'Dowd, C., Monahan, C., and Dall'Osto, M.: On the occurrence of open ocean particle production and growth events, *Geophys. Res. Lett.*, 37, L19805, doi:10.1029/2010GL044679, 2010.
- Pierce, J. R., Westervelt, D. M., Atwood, S. A., Barnes, E. A., and Leitch, W. R.: New-particle formation, growth and climate-relevant particle production in Egbert, Canada: analysis from 1 year of size-distribution observations, *Atmos. Chem. Phys.*, 14, 8647-8663, 10.5194/acp-14-8647-2014, 2014.
- Stohl, A.: Computations, accuracy and applications of trajectories - A review and bibliography, *Atmos. Environ.*, 32, 947-966, 1998.
- Ström, J., Engvall, A.-C., Delbart, F., Krejci, R., and Treffeisen, R.: On small particles in the Arctic summer boundary layer: observations at two different heights near Ny-Ålesund, Svalbard, *Tellus B - Chemical and Physical Meteorology*, 61, 473-482, 2009.
- Venzac, H., Sellegri, K., Villani, P., Picard, D., and Laj, P.: Seasonal variation of aerosol size distributions in the free troposphere and residual layer at the Puy de Dôme station, France, *Atmos. Chem. Phys.*, 9, 1465-1478, 10.5194/acp-9-1465-2009, 2009.
- Yli-Juuti, T., Riipinen, I., Pasi, A., Nieminen, T., Maenhaut, W., Janssens, A., Claeys, M., Salma, I., Ocskay, R., Hoffer, A., Imre, K., and Kulmala, M.: Characteristics of new particle formation events and cluster ions at K-pusztá, Hungary, *Boreal Environment Research*, 14, 2009.
- Young, L. H., Lee, S. H., Kanawade, V. P., Hsiao, T. C., Lee, Y. L., Hwang, B. F., Liou, Y. J., Hsu, H. T., and Tsai, P. J.: New particle growth and shrinkage observed in subtropical environments, *Atmos. Chem. Phys.*, 13, 547-564, 10.5194/acp-13-547-2013, 2013.

1  
2  
3  
4  
5  
6  
7  
8  
9  
10  
11  
12  
13  
14  
15  
16

## New particle formation in the Svalbard region 2006 - 2015

Jost Heintzenberg<sup>1</sup>, Peter Tunved<sup>2</sup>, Martí Galí<sup>3</sup>, and Caroline Leck<sup>4</sup>

1: Leibniz Institute for Tropospheric Research (TROPOS), Permoserstr. 15, 04318 Leipzig, Germany

2: Department of Environmental Science and Analytical Chemistry (ACES), Stockholm University, 10691 Stockholm, Sweden

3: Takuvik Joint International Laboratory & Québec-Océan, Université Laval, G1V 0A6 Québec, Canada

4: Department of Meteorology, Stockholm University (MISU), 10691 Stockholm, Sweden

rev. 2017-2-18 10:48  
**Gelöscht:** Applied

rev. 2017-2-18 10:48  
**Gelöscht:** ,

rev. 2017-2-18 10:48  
**Gelöscht:** (MISU),

20 Abstract

21

22 Events of new particle formation, (NPF), were analyzed in a ten-year data set of hourly  
23 particle size distributions recorded on Mt. Zeppelin, Spitsbergen, Svalbard. Three different  
24 types of NPF-events were identified through objective search algorithms. The first and  
25 simplest algorithm utilizes short-term increases in particle concentrations below 25 nm,  
26 (PCT-events). The second one builds on the growth of the sub-50 nm diameter-median,  
27 (DGR-events), and is most closely related to the classical “banana-type” of events. The third  
28 and most complex, so-called multiple-size approach to identifying NPF-events builds on a  
29 hypothesis suggesting the concurrent production of polymer gel particles at several sizes  
30 below about 60 nm, (MEV-events).

31 As a first and general conclusion we can state that NPF-events are a summer phenomenon  
32 and not related to Arctic haze, which is a late winter-to-early spring feature. The occurrence  
33 of NPF-events appears to be somewhat sensitive to the available data on precipitation. The  
34 seasonal distribution of solar flux suggests some photochemical control that may affect  
35 marine biological processes generating particle precursors and/or atmospheric photochemical  
36 processes that generate condensable vapors from precursor gases. Notable, the seasonal  
37 distribution of the biogenic methanesulfonate, (MSA), follows that of the solar flux although  
38 it peaks before the maxima in NPF-occurrence.

39 A host of ancillary data and findings point to varying and rather complex marine biological  
40 source processes. The potential source regions for all types of new particle formation appear  
41 to be restricted to the marginal ice and open water areas between Northeastern Greenland and  
42 Eastern Svalbard. Depending on conditions yet to be clarified new particle formation may  
43 become visible as short bursts of particles around 20 nm, (PCT-events), longer events  
44 involving condensation growth, (DGR-events), or extended events with elevated  
45 concentrations of particles at several sizes below 100 nm, (MEV-events). The seasonal

rev. 2017-2-18 10:48

Gelöscht: event.

rev. 2017-2-18 10:48

Gelöscht: appear

rev. 2017-2-18 10:48

Gelöscht: Whereas

49 distribution of NPF-events peaks later than that of MSA and, DGR and in particular of MEV-  
50 events reach into late summer and early fall with much open, warm, and biologically active  
51 waters around Svalbard. Consequently, a simple model to describe the seasonal distribution  
52 of the total number of NPF-events can be based on solar flux, and sea surface temperature,  
53 representing environmental conditions for marine biological activity, and condensation sink,  
54 controlling the balance between new particle nucleation and their condensational growth.  
55 Based on the sparse knowledge about the seasonal cycle of gel-forming marine  
56 microorganisms and their controlling factors we hypothesize that the seasonal distribution of  
57 DGR and more so MEV-events reflect the seasonal cycle of the gel-forming phytoplankton.

58

59

## 60 1. Introduction

61

62 In the late 1970ies and early 1980ies the interest in the Arctic atmospheric aerosol widened  
63 from the well-identified winter phenomenon of Arctic haze (Rahn and Shaw, 1977;  
64 Heintzenberg and Leck, 1994) to summer conditions in this northernmost remote region. In  
65 the pristine Arctic summer air the so-called background aerosol (Junge, 1963) was expected  
66 to be most clearly visible, far away from the northern hemispheric anthropogenic emission  
67 centers at lower latitudes. Episodic and localized occurrences of high concentrations of  
68 ultrafine particles, (here defined as particles with diameters < 100 nm), in the summer Arctic  
69 were explained by rare import of polluted air from lower latitudes (Flyger and Heidam, 1978;  
70 Heintzenberg and Larssen, 1983) or hypothetical anthropogenic sources in the Arctic  
71 (Jaenicke and Schütz, 1982).

72 With the advent of sensitive condensation nuclei counters (Agarwal and Sem, 1980) and  
73 differential mobility analyzers (Knutson and Whitby, 1975b, a), more details became visible in  
74 the Arctic sub-micrometer aerosol. High numbers of ultrafine particles were observed in  
75 connection with fog passages (Lannefors et al., 1983) and chemical aerosol information  
76 indicated a regional – possibly biogenic – particle sources in the summer Arctic  
77 (Heintzenberg, 1989). The high molar ratios of methane sulfonate, (MSA), to non-sea salt  
78 sulfate, ( $\text{nssSO}_4^{2-}$ ), of 0.28 in the Arctic summer aerosol found by Heintzenberg and Leck  
79 (1994) substantiated the biogenic source of the particles.

80 The establishment of long-term Arctic aerosol monitoring at the fringes of the pack ice in  
81 Alaska (e.g., Polissar et al., 1999), Canada (e.g., Norman et al., 1999; Willis et al., 2016), and  
82 on Spitsbergen (e.g., Tunved et al., 2013), revealed more details of potential sources of the  
83 summer aerosol, in particular their connection to the marine biosphere in the Arctic. The  
84 unique series of systematic aerosol studies in the central Arctic north of 80°N onboard the  
85 Swedish icebreaker *Oden* in 1996 led to the formulation of a new hypothesis concerning a

rev. 2017-2-18 10:48

Gelöscht: (Knutson and Whitby, 1975a, b)

rev. 2017-2-18 10:48

Gelöscht: (e.g., Tunved et al., 2013)



88 specific process of marine biogenic particle formation (Leck and Bigg, 1999). The marine  
89 biogenic particles involved behaved as polymer gels and originated in the surface microlayer  
90 (SML) of the ocean, (Orellana et al., 2011b), from the activity of sea-ice algae,  
91 phytoplankton and, perhaps, bacteria. The new particle events were reported to occur as  
92 simultaneous enhancement of particle number concentrations in the whole size-range below  
93 50 nm, and not with the prototypical “banana growth” (Kulmala et al., 2004). Two more  
94 *Oden* cruises in 2001 and 2008 yielded results that were partly contradicting (Held et al.,  
95 2011b; Held et al., 2011a), partly supporting the SML hypothesis (Leck et al., 2013; Karl et  
96 al., 2013; Orellana et al., 2011b; Leck and Bigg, 2010). The synopsis of the results of four  
97 *Oden* cruises of Heintzenberg et al. (2015) identified geographic regions of new particle  
98 formation (NPF) in the inner Arctic while stressing the importance of recent open water and  
99 related biological activity in the sea in transects by air masses with new particle formation  
100 over the central Arctic.

101 Two years of aerosol size distributions from Mt. Zeppelin, Spitsbergen and Alert, both  
102 located at the fringes of the central pack ice, were analyzed by Croft et al. (2016a) with a  
103 global aerosol geophysics model. They discuss classical new-particle nucleation, coagulation  
104 scavenging in clouds, scavenging by precipitation, and transport in order to explain the annual  
105 cycle of the Arctic aerosol. Croft et al. (2016a) find two seasonal maxima in their modeled  
106 particle nucleation rates, one in March, and one in July. In spring, their simulated NPF occurs  
107 mainly in the free troposphere, whereas in summer, it occurs also in the planetary boundary  
108 layer. More recently, Croft et al. (2016b) state that ammonia from seabird-colony guano is a  
109 key factor contributing to bursts of newly formed particles, which are observed every summer  
110 in the near-surface atmosphere, at least at Alert, Nunavut, Canada. Earlier, the results of  
111 studies with another global aerosol model by Browse et al. (2014) suggested that the potential  
112 increase in NPF in the Arctic with potential increases in cloud condensation nuclei is

113 compensated by wet scavenging. They also state that scavenging by pre-existing large  
114 particles suppresses NPF-events.

115 Based on three years of data from the two Arctic sites Thule and Ny-Ålesund (gruvebadet)  
116 Becagli et al. (2016) examined the sources and environmental factors controlling the  
117 biological aerosol component MSA. Their analysis included satellite-derived Chlorophyll-*a*  
118 (an indicator of phytoplankton biomass), oceanic phytoplankton primary productivity, (PPP),  
119 and sea ice. Whereas they found good correlations between MSA, PPP and sea ice, (the latter  
120 two being closely related), their data did not allow any statements on NPF processes.

121 To date the longest record of sub-micrometer number-size distributions of the Arctic  
122 aerosol down to 5 nm particle diameter and below has been accumulated on Mt. Zeppelin,  
123 Spitsbergen (Tunved et al., 2013; Heintzenberg and Leck, 1994). For the ten years from 2006  
124 through 2015 a total of 63936 quality-controlled hours of aerosol data are available, i.e.  
125 during 73% of all hours of the ten years. In the present study we exploit this formidable data  
126 set in a search for processes forming new particles. An important first step in this work was  
127 formulating completely objective criteria for the identification of events. In the relatively  
128 clean Arctic environment we do not expect the classical nucleation and growth events as  
129 frequently observed over the continents, (cf. Kulmala et al., 2004), to dominate. Thus, we  
130 refrained from applying the objective search algorithm formulated by Heintzenberg et al.,  
131 (2007) for this “Banana-type” of events. Instead we formulated new objective search  
132 algorithms allowing several potential types of new particle formation events or formation  
133 processes. With a host of complementary atmospheric and surface physical, chemical, and  
134 biological information a large number of NPF-events identified with these algorithms will be  
135 analyzed in the following chapters.

136

137

138

139 **2. Database**

140

141 The Mt. Zeppelin observatory

142

143 Situated at the top of Mt Zeppelin, Svalbard (78° 56'N, 11° 53'E), the Zeppelin observatory  
144 offers a unique possibility to study the characteristic features of Arctic atmospheric  
145 constituents such as trace gases and aerosol particles. At a height of 474 m a.s.l. the station is  
146 located near the top of the local planetary boundary layer and represents remote Arctic  
147 conditions. The closest source of pollution, the small community of Ny-Ålesund, is located  
148 ~2 km north of the station  
149 ([http://www.esrl.noaa.gov/psd/iasoa/sites/default/files/stations/nyalesund/nyalesund\\_site.jpg](http://www.esrl.noaa.gov/psd/iasoa/sites/default/files/stations/nyalesund/nyalesund_site.jpg)).

150 However, the elevation difference and typical wind patterns largely prevent pollution from  
151 nearby sources to reach the Zeppelin Observatory. The dominating wind pattern is east-  
152 southeast katabatic flow from Kongsvegen glacier or from northwesterly directions as  
153 channeled by the Kongsfjord (Beine et al., 2001; Heintzenberg et al., 1983). The station itself  
154 was initially established in 1991, and is owned by the Norwegian Polar Research Institute  
155 (NP). The Norwegian Institute for Air Research (NILU) is responsible for the coordination of  
156 the scientific program.

157

158

159 **2.1 Physical aerosol data**

160

161 After a period of continuous aerosol measurements by the Department of Meteorology,  
162 Stockholm University in the early 1990ties, (Heintzenberg and Leck, 1994), the Department  
163 of Analytical Chemistry and Environmental Science, Stockholm University, initialized  
164 observations of the aerosol number size distribution in mid-2000. Originally, the system

165 consisted of a single differential mobility analyzer system, (DMPS), consisting of a medium-  
166 size Hauke-type differential mobility analyzer, (DMA), together with a TSI 3760  
167 condensation particle counter, covering diameters between 20 and ~500nm. From 2006 on  
168 the particle size range was widened covering particle sizes between 10 and 790 nm. In 2005,  
169 the rain-cover over the inlet was replaced. Initially, the instrument inlet was of a PM10 type,  
170 removing particles or hydrometeors with diameters  $>10\ \mu\text{m}$  from the sampled air stream.  
171 During a substantial renewal of the Stockholm University equipment in 2010-2011, both inlet  
172 and DMPS system were replaced.

173 Since then, the DMPS-system utilizes a custom-built twin DMA-setup comprising one  
174 Vienna-type medium DMA coupled to a TSI CPC 3010 covering sizes between 25-800 nm  
175 and a Vienna-type long DMA coupled with at TSI CPC 3772 covering sizes between 5-60  
176 nm. The size distributions from the two systems are harmonized on a common size grid and  
177 then merged. Both systems use a closed-loop flow setup. The current inlet hat is of whole air  
178 type, complying with EUSAAR<sup>1</sup> standard for high altitude or Arctic sampling conditions. In  
179 the current setup, the inlet is operated with a flow of ca. 100 liters per minute, (lpm). Laminar  
180 flow conditions apply throughout the sampling lines. Outside of the station, the inlet  
181 temperature is kept above 0°C using active heating. Inside the station the temperature  
182 increases gradually to room temperature (maximum temperature reaches ca. 25 °C, but  
183 remains typically around 20°C). Relative humidity, (RH) and temperature are internally  
184 monitored and measurements are maintained at dry conditions with  $\text{RH} < 30\%$ . The system is  
185 regularly checked with latex spheres and flow controls. The recorded data are manually  
186 screened and crosschecked with other available observation as in Tunved et al. (2013). If  
187 inconsistencies were found between the different datasets, further investigation was

---

<sup>1</sup> EUSAAR (European Supersites for Atmospheric Aerosol Research) is an EU-funded I3 (Integrated Infrastructures Initiatives) project carried out in the FP6 framework of the specific research and technological development gram "Structuring the European Research Area - Support for Research Infrastructures", (<http://www.eusaar.net/>).

rev. 2017-2-18 10:48

Gelöscht: (2013).

189 performed to exclude data that were identified as affected by instrumental errors. Using the  
190 instrumental logbook, periods of local activity potentially influencing the sampling were also  
191 excluded from the dataset. During the years 2006 – 2010 no particles below ten nanometers  
192 in diameter were recorded. From 2011 on four more diameter bins down to 5 nm were  
193 included and a different diameter array was utilized. To allow for a synopsis of all years all  
194 size distributions were interpolated on the pre-2011 diameter array and all integrals of the size  
195 distribution over particle diameter were taken over the joint diameter range 10 to 631 nm. For  
196 the pre-2011 years the data at the four size channels below 10 nm were flagged as missing.  
197 However, whenever results cover the complete time series the resulting number  
198 concentrations in the four first channels covering the years 2011 – 2015 are carried along.

199 For the identification of NPF in terms of particle growth the parameter D50 in nanometer  
200 was calculated as the number median diameter of particles smaller than 50 nm but larger than  
201 10 nm, i.e. 50% of all particles below that size are smaller than D50. Besides this parameter  
202 Table 1 lists nine integral particle parameters, which are utilized in the NPF-search  
203 approaches or in the interpretation of results. These aerosol parameters quantify total particle  
204 number, (NTO), and particle numbers in sub-ranges of the number size distribution such as  
205 N25, quantifying the total number of particles between ten and 25 nm.

206 Following the concept developed by Pirjola et al., (1999), and Kulmala et al., (2001) we  
207 calculated the condensation sink, (CS,  $s^{-1}$ ), as a parameter with which the probability of new  
208 particle formation from the gas phase and the necessary amount of condensable vapor can be  
209 estimated. We utilized number size distributions, pressure and temperature taken from our  
210 database for this calculation.

rev. 2017-2-18 10:48

**Gelöscht:** For this calculation we

rev. 2017-2-18 10:48

**Gelöscht:** from our database

211  
212  
213  
214

## 217 2.2 Chemical aerosol data

218

219 For the interpretation of NPF-events we employed chemical information derived from the  
220 analyses of high volume particle samples taken by the Norwegian Institute for Air research,  
221 (NILU). A high volume sampler (PM10) was used to collect samples for a quantitative  
222 determination of sodium, ( $\text{Na}^+$ ), sulfate, ( $\text{SO}_4^{2-}$ ) and MSA ( $\text{CH}_3\text{SOO}^-$ ). The sampler collected  
223 material for analysis in one to three days. Blank samples were obtained by mounting the  
224 glass fiber filters at the sampling site with the same sampling period but without air passing  
225 through.  $\text{Na}^+$  and  $\text{SO}_4^{2-}$  were analyzed by NILU and have been downloaded for the present  
226 study from the EBAS database (<http://ebas.nilu.no>), which list details about the sampling  
227 technique and the sampling protocol. ~~Nss  $\text{SO}_4^{2-}$  was determined from total sulfate correcting~~  
228 ~~for sea salt sulfate, as  $0.25 \times \text{Na}^+$~~  (Keene et al., 1986).

229 MSA was analyzed at the laboratory of the Department of Meteorology, Stockholm  
230 University. To allow for subsequent chemical determinations the ambient samples and blanks  
231 were carefully handled in a glove box (free from particles, sulfur dioxide and ammonia). At  
232 the time of the chemical analyses, still in the glove box, the substrates were extracted (in  
233 centrifuge tubes) with  $60 \text{ cm}^3$  deionized water (Millipore Alpha-Q, conductivity  $18 \text{ M}\Omega\text{cm}$ ).  
234 The extracts were thereafter analyzed for weak anions by chemically suppressed ion  
235 chromatography (IC, Dionex ICS-2000) using Dionex AG11/AS11 columns. In order to trap  
236 carbonates and other ionic contaminants a Dionex ATC-1 column was used before the  
237 injection valve. The injection volume was  $50 \mu\text{dm}^3$ . Quality checks of the IC-analyses were  
238 performed with both internal and external reference samples (Das et al., 2011). The analytical  
239 detection limits obtained for the various ions, defined as twice the level of peak-to-peak  
240 instrument noise, was  $0.0001 \mu\text{eq dm}^{-3}$  for MSA. The overall analytical accuracy was better  
241 than 1.5%.

242

rev. 2017-2-18 10:48

Gelösch: \*)

rev. 2017-2-18 10:48

Gelösch: To be able to apportion the measured

rev. 2017-2-18 10:48

Gelösch: to nss $\text{SO}_4^{2-}$  the observed concentrations of  $\text{Na}^+$  were used

rev. 2017-2-18 10:48

Gelösch: the reference element based on the assuming that all  $\text{Na}^+$  is of marine origin,

250 **2.3 Back-trajectories and meteorological data**

251

252 For every hour during the ten years 2006 through 2015 three-dimensional back trajectories  
253 have been calculated arriving at 474 m at Mt. Zeppelin. The trajectories have been calculated  
254 backward for up to ten days using the HYSPLIT4 model (Draxler and Rolph, 2003) with  
255 meteorological data from the Global Data Assimilation System with one-degree resolution  
256 (GDAS1). Trajectories extending backwards for ten days are inaccurate at origin due to the  
257 trajectory uncertainty of 25-30% of its length, (Stohl, 1998). More information about the  
258 GDAS dataset can be found at Air Resources Laboratory (ARL), NOAA  
259 (<http://ready.arl.noaa.gov>), from which the meteorological data were downloaded.

260 During the analyzed time period meteorological records at the Mt. Zeppelin station are  
261 rather limited in quality and were frequently interrupted. There are no precipitation  
262 measurements and wind measurements are strongly influenced by the station building and by  
263 the local topography. In order to have an internally consistent, and unbroken meteorological  
264 record we utilized hourly meteorological parameters at trajectory arrival times as calculated  
265 by the HYSPLIT4 model. We emphasize that their accuracy depends on the quality of the  
266 meteorological model inside HYSPLIT4 and the accuracy and representativeness of the  
267 meteorological fields utilized by the model. Of the local meteorological record air  
268 temperature was considered the most reliable and thus explored in a comparison of trajectory  
269 calculated and modeled meteorological data. When comparing the 42600 contiguous hourly  
270 records from 2008-01-01 until 2012-11-10 the average ratio of measured and calculated  
271 temperatures is 0.98, with a coefficient of determination of 0.96. The utilized model  
272 parameters are listed in Table 1.

273 As an additional parameter we evaluated the vertical air movement of the trajectories  
274 during the last hour before arrival by subtracting the trajectory height one hour before arrival

rev. 2017-2-18 10:48

Gelöscht: the

276 at the arrival height of 474 meter. The resulting vertical displacement parameter, DZ, is given  
277 in meters per hour. Positive values of DZ indicate a lifting of the air.

278 The most important missing meteorological information concerns the local cloud cover.  
279 No direct recording was available of times during which the station was in clouds. The  
280 closest available cloud instrument is a ceilometer operated by the Alfred Wegener Institute  
281 (AWI) at their Koldewey Station in Ny-Ålesund, i.e. in the valley below Mt. Zeppelin, some  
282 2.8 km of horizontal distance from the position of the mountain station. From the one-minute  
283 records of the ceilometer we derived hourly values of the 25% percentile of cloud base, which  
284 was used as an indicator for the Zeppelin station being in cloud. This ceilometer parameter is  
285 listed as C25 in Table 1.

286 Precipitating clouds scavenge the planetary boundary layer and thus reduce the available  
287 particle surface as condensation sink of particle precursors. As a consequence nucleation  
288 from the gas phase may be facilitated (Tunved et al., 2013). As in Tunved et al. (2013) we  
289 utilized the HYSPLIT-modeled precipitation along the back trajectories. Sums of  
290 precipitation, (SP, see Table 1), were calculated along each back trajectory and will be  
291 referred to as SP1 (during the last day), SP2 (during the last but one day), and SP5 (during  
292 days three to five) before arrival at Mt. Zeppelin.

293

294

## 295 2.4 Marine biological data

296

297 The biologically active marginal ice zone is a major natural source of sulfur in the Arctic  
298 summer atmosphere, (Leck and Persson, 1996b, a), and Wiedensohler et al. (1996), indicated  
299 a potentially important role of dimethyl sulfide (DMS) in regional new particle formation.  
300 DMS emissions from the sea have long been proposed to control new particle formation in the  
301 marine boundary layer, (Charlson et al., 1987), which builds on DMS<sub>aq</sub> being transported via

rev. 2017-2-18 10:48

Gelösch: cloudiness

rev. 2017-2-18 10:48

Gelösch: clouds. The meteorological parameters are

rev. 2017-2-18 10:48

Gelösch: . Precipitating clouds scavenge the planetary boundary layer and thus reduce the available particle surface for condensational uptake of particle precursors. As a consequence nucleation from the gas phase may be facilitated (Tunved et al., 2013). As in Tunved et al. (2013) we utilized the HYSPLIT-modeled precipitation along the back trajectories. Sums of precipitation, (SP, see Table 1), were calculated along each back trajectory and will be referred to as SP1 (during the last day), SP2 (during the last but one day), and SP5 (during days three to five) before arrival at Mt. Zeppelin.



319 turbulence and diffusion to the sea-air interface, represented by the transfer velocity, which in  
320 turn depends on sea-surface temperature, salinity, and wind speed, (Liss and Merlivat, 1986).

321 | Once in the atmosphere  $\text{DMS}_g$  is photochemical oxidized via intermediates such as sulfuric  
322 acid and methane sulfonic acid, (Ayers et al., 1996), which eventually leads to the formation  
323 of aerosol  $\text{nssSO}_4^{2-}$  and MSA. The products of the photochemical oxidation of DMS the ratio  
324 MSA/  $\text{nssSO}_4^{2-}$  show a temperature dependence (Bates et al., 1990), favoring MSA in the cold  
325 Arctic environment (Karl et al., 2007).

326 Dimethyl sulfide in the ocean ( $\text{DMS}_{aq}$ ) is produced through the degradation of its algal  
327 precursor dimethylsulfoniopropionate (DMSP) by microbial food webs, (Simó, 2001). At  
328 high latitudes, total DMSP (DMSPt) and therefore  $\text{DMS}_{aq}$ , essentially follows the seasonal  
329 cycle of phytoplankton biomass, (Lana et al., 2012). DMSPt is defined as the sum of  
330  $\text{DMSP}_{dissolved}$  and  $\text{DMSP}_{particulate}$  concentration. Yet, the amount of DMSPt per unit  
331 phytoplankton biomass may vary depending on species composition and physiological state,  
332 (Keller et al., 1989).

333 The dissolved organic carbon (DOC) concentrations in surface waters of the high Arctic  
334 Ocean are up to ten times higher than in any other ocean basin and closer in range to DOC  
335 levels reported for sea ice (Gao et al., 2012). A large fraction of DOC spontaneously  
336 assembles into polymer gels: polysaccharide forming hydrated calcium bonded three-  
337 dimensional networks to which other organic compounds, such as proteins and lipids, are  
338 readily bound. The assembly and dispersion of the polysaccharide molecules can be affected  
339 by environmental parameters, such as UV-B radiation (280-320nm) dispersing or inhibiting  
340 gel formation, and/or pH and temperature inducing gel volume phase changes (swelling and  
341 shrinkage). In the study of Orellana et al., (2011b), the swelling and shrinking of the  
342 polysaccharide networks or polymer gels were also causally related by additions of nano to  
343 micromolar levels of DMS and DMSP. High DMSP concentrations have also been measured

rev. 2017-2-18 10:48

Gelöscht: ventilated to

345 in the mucilage surrounding prymnesiophyte *Phaeocystis pouchetii* colonies in Arctic waters,  
346 representing up to 25% of the total water column DMSP pool, (Matrai and Vernet, 1997).  
347 The findings made by Orellana et al., (2011b) were in agreement with previous findings by  
348 Orellana et al., (2011a) that high concentrations of DMSP and DMS are stored in the acidic  
349 secretory vesicles of the *Phaeocystis* algae where DMSP is trapped within the condensed  
350 polyanionic gel matrix until the secretory vesicles are triggered by environmental factors such  
351 as temperature to release gels that undergo volume phase transition and expand at the higher  
352 pH of seawater. Exocytosis of polymer gels accompanied by elevated DMS and DMSP  
353 concentrations suggests the transport of these chemical compounds by the gel matrix.  
354 Schoemann et al., (2005) report that *Phaeocystis antarctica* is particularly well adapted to low  
355 temperatures, being more competitive than *P. pouchetii* for temperatures between -2 and  
356 +2 °C. *Phaeocystis pouchetii*, however, appears to be better adapted to temperatures closer to  
357 5 °C. In the Arctic a higher occurrence of the *Phaeocystis pouchetii* would be expected in the  
358 northward advection of warm Atlantic water masses around Svalbard.

359 Here we estimated DMSPt at the sea surface using the algorithm described by Galí et al.  
360 (2015). The DMSPt algorithm exploits the distinct relationship between DMSPt and  
361 Chlorophyll-*a* depending on the light exposure regime of the phytoplankton community. The  
362 light exposure regime is defined by the ratio between euphotic layer depth and mixed layer  
363 depth ( $Z_{eu}/MLD$ ). Additional predictor variables used are sea surface temperature (SST) and  
364 particulate inorganic carbon (PIC), which is used in the algorithm as a proxy for  
365 coccolitophores such as *Emiliania huxleyi*. During late bloom stages, the calcite plates that  
366 cover coccolitophore cells (called coccoliths) detach and cause an increase in seawater  
367 backscatter that invalidates satellite retrievals of Chlorophyll-*a*. Therefore, inclusion of PIC  
368 in the algorithm as a proxy for DMSPt increases data coverage. Although the algorithm was  
369 developed for the global ocean, validation results with in situ data indicate that it performs as  
370 well or slightly better in Arctic and sub-Arctic waters.

371 The use of remotely sensed DMS<sub>Pt</sub> as a proxy for marine DMS<sub>aq</sub> emission is a significant  
372 improvement with respect to prior studies that used Chlorophyll-*a* (Becagli et al., 2016;  
373 Zhang et al., 2015). Yet, it is not ideal because (i) the ratios DMS<sub>aq</sub>/DMS<sub>Pt</sub> in surface  
374 seawater are variable, and tend to be higher in high solar irradiance and nutrient-poor  
375 conditions typical of summer, (Gali and Simó, 2015), and (ii) even if DMS<sub>Pt</sub> is a better proxy  
376 for DMS<sub>aq</sub>, the influence of meteorological and sea surface conditions (mainly wind speed  
377 and SST) on the sea-air flux of DMS<sub>aq</sub> is not taken into account. Development is underway of  
378 an algorithm for the retrieval of DMS<sub>g</sub> concentrations in air and DMS fluxes.

379 The DMS<sub>Pt</sub> algorithm was run for the 2006-2015 period using daily composites of the  
380 Moderate Resolution Imaging Spectroradiometer on the Aqua satellite (MODIS-Aqua) at 4.64  
381 km resolution (L3BIN, reprocessing R2014.0) downloaded from NASA's Ocean Color  
382 website (<http://oceancolor.gsfc.nasa.gov>). The MODIS variables used include Chlorophyll-*a*  
383 concentration derived with the GSM algorithm, (Maritorena et al., 2002), PIC, nighttime SST  
384 and Z<sub>eu</sub>. MODIS nighttime SST was complemented with SST from the Advanced Very High  
385 Resolution Radiometer (AVHRR, <https://podaac.jpl.nasa.gov/AVHRR-Pathfinder>) to increase  
386 data availability. MLD was obtained from the MIMOC climatology, (Schmidtko et al.,  
387 2013), which was linearly interpolated from its original 0.5°x0.5° grid at monthly resolution  
388 to the MODIS grid at daily resolution.

389 Satellite remote sensing of biological activity in surface waters requires ice-free and at  
390 least part of the time cloud-free. The passive sensing methods of MODIS additionally require  
391 a minimum of solar illumination of the scenes (i.e., solar zenith angle < 70°; (IOCCG, 2015)).  
392 Consequently, the length of the satellite-observable period used to compute DMS<sub>Pt</sub> means  
393 shortens from all-year-round at latitudes <45° to approximately six months (the spring-  
394 summer semester) at 80°N. In addition, the annual DMS<sub>Pt</sub> map in Fig. 3 excludes all land and  
395 ice covered regions. In order to increase data coverage, daily DMS<sub>Pt</sub> composites were binned  
396 to five-day periods and a 46.4 km equal-area sinusoidal grid, (10x10 bins of the original pixel

397 size). The average distance between a trajectory point and the closest center of a MODIS  
398 pixel is 18 km.

399 Following the same approach as with the ice data average DMSPt from ocean color data,  
400 (OC), along each back trajectory were calculated and will be referred to as OC1 (the last day),  
401 OC2 (the last but one day), and OC5 (days three to five) before arrival at Mt. Zeppelin. In  
402 this procedure missing data were flagged as such, and were not taken into account.

403

404

## 405 **2.5 Ice data**

406

407 For the interpretation of events of new particle formation observed during the *Oden* cruises  
408 information on pack ice extent under the air masses reaching the sampling points proved  
409 crucial (Heintzenberg et al., 2015). Another motivation for utilizing ice data in the present  
410 study is the fact that the Svalbard region experiences large seasonal changes in pack ice cover  
411 which we expect to have strong effects on emissions of particles and their precursor gases.  
412 Thus daily ice concentrations were taken from the NSIDC database (<https://nsidc.org/data>).  
413 The irregularly shaped data gap around the pole caused by the inclination of satellite orbits  
414 and instrument swath was filled with 100% cover. To each hourly position and data of the  
415 back trajectories the ice information in the corresponding maps of ice concentrations were  
416 added and displayed in Fig. 2. On average the closest pixel in the ice maps was about 12 km  
417 off any trajectory point.

418 In the discussion of results we utilize the complement of ice cover, i.e., the amount of open  
419 water because the marine biological processes of interest predominantly take place in the  
420 open water, (Leck and Persson, 1996a). As integral parameters average open water, (OW),  
421 percentages along each back trajectory were calculated and will be referred to as OW1 (the  
422 last day), OW2 (the last but one day), and OW5 (days three to five) before arrival at Mt.

423 Zeppelin. The most solid ice cover is seen in an area reaching from Northeastern edge of  
424 Greenland via North Pole to Parry Island. A marginal ice zone extends along the east coast of  
425 Greenland to Franz-Josef-Land, and the area between Svalbard and the latter island.

426

427

## 428 **2.6 ERA-Interim data of sea surface temperature**

429

430 Daily Sea Surface Temperature (SST) data for our study period (2006-2015) were  
431 downloaded from the website of the European Centre for Medium-Range Weather Forecasts  
432 (ECMWF). A description of the global atmospheric reanalysis, (ERA-Interim), has been  
433 given by Dee et al. (2011), and a guide to the products and the download procedures can be  
434 found at <http://www.ecmwf.int/en/elibrary/8174-era-interim-archive-version-20>. Briefly,  
435 ERA-Interim is an assimilating model reanalysis of the global atmosphere and sea-surface  
436 physical parameters covering the data-rich period since 1979. SST data were downloaded at a  
437 resolution of approximately  $0.56^\circ$  and regridded onto the same 46 km equal-area sinusoidal  
438 grid used for DMSP and cloud fraction, (see below). Ice-covered pixels were screened out  
439 prior to the back-trajectory analysis. In the Arctic region, ERA-Interim has been shown to be  
440 a top performer among a number of atmospheric reanalyses, (Lindsay et al., 2014).

441

442

## 443 **2.7 MODIS cloud fraction**

444

445 Persistent cloud cover limits PPP in Arctic and Sub-arctic seas, (Bélanger et al., 2013), and,  
446 as mentioned above, irradiance at the sea surface, which is largely controlled by cloudiness,  
447 influences  $\text{DMSP}_{\text{dissolved-to-DMS}_{\text{aq}}}$  conversion. Boundary layer clouds are known to be  
448 additional controllers of the surface aerosol (Heintzenberg, 2012). In the summer Arctic low

449 level clouds and fogs are widespread (Warren and Hahn, 2002). Both scavenging and new  
450 particle formation have been observed in connection with low clouds and fog passages  
451 (Lannefors et al., 1983; Heintzenberg and Leck, 1994; Leck and Bigg, 1999; Heintzenberg et  
452 al., 2006; Karl et al., 2013). Beyond the cloud base derived from the ceilometer we have no  
453 other in situ local or regional cloud information. Thus, we utilize satellite-derived cloud  
454 information.

455 Daily Level-3 global cloud fraction with one-degree resolution was downloaded from  
456 NASA website (<http://modis-atmos.gsfc.nasa.gov>, Hubanks et al., 2015) and extracted for our  
457 region of interest. Briefly, level 3 images correspond to the aggregation of all level 2 images  
458 (1 km resolution) available within the one-degree resolution grid. For a given L2 scene, each  
459 pixel is assigned a value of 1 (cloudy) or zero (clear sky), and then the individual scene values  
460 are averaged over a 24-hour period. Note that a given pixel can be revisited up to six or seven  
461 times in the course of a day at high latitudes. Finally, the daily composites were re-projected  
462 to 46.4 km pixels to match the spatial resolution of DMSPt. The average distance between a  
463 trajectory point and the closest MODIS pixel was 18 km.

464 The cloud fraction CF as well as other cloud properties from MODIS have been  
465 extensively used, for instance to study the global spatial and temporal distribution of clouds  
466 over the last decade (e.g., King et al., 2013). Several studies have also successfully  
467 performed validation by comparison with in situ data (e.g., An and Wang, 2015) which  
468 demonstrated the ability of the MODIS-aqua sensor to retrieve cloud cover.

469 Following the same approach as with the ice data and DMSPt, average cloud fractions,  
470 (CF, see Table 1), along each back trajectory were calculated and will be referred to as CF1  
471 (the last day), CF2 (the last but one day), and CF5 (days three to five) before arrival at Mt.  
472 Zeppelin. Missing data are flagged as was done with DMSPt data.

473

474

### 475 3. Three approaches to identifying events of new particle formation

476

477 There are no definitive and no generally accepted methods to identify or predict NPF-events  
478 in atmospheric time series of aerosol data. Thus, in the present study we explored different  
479 approaches with varying degrees of complexity to identify such events. We emphasize that  
480 none of these approaches explicitly is connected to diel cycles such as in Dal Maso et al.,  
481 (2005) or makes any assumptions about the time of day during which new particle formation  
482 occurs. Three objective search algorithms were written in FORTRAN to analyze the time  
483 series of hourly records of aerosol parameters in search of new particle formation:

484 1. The simplest approach of upper percentiles (PCT-approach), assumes that NPF-events are  
485 characterized by extremely high concentrations of small particles in terms of N25 (see  
486 Table 1). The key parameter characterizing each PCT-event was the value of N25  
487 averaged over a fixed number of hours, ( $N25_{av}$ ), after the nominal start of an event, (see  
488 below). With  $N25_{av}$  also a nominal length of PCT-events was defined as the number of  
489 hours after the start of an event by which N25 sank to less than half of  $N25_{av}$ .

490 2. The more specific approach of diameter growth (DGR-approach) builds on the temporal  
491 development of the particle size distribution in terms of a systematic growth of the  
492 diameter D50 (see section 4.1) to find the classical “Banana Type” of NPF-event,  
493 (Kulmala et al., 2004). The key parameter characterizing each DGR-event was the average  
494 growth of D50 during the nominal event length NUC, (see below). For this approach the  
495 nominal length of events was reached when the running two-hour average growth fell  
496 below the value one.

497 2. The most complex approach of multiple-size events, (MEV-approach), searches for events  
498 with concurrent appearance of concentration increases in several size classes below 60 nm  
499 diameter (Karl et al., 2013; Leck and Bigg, 2010). The key parameter characterizing each  
500 MEV-event was the relative concentration increase averaged over the chosen size classes

501 below 60 nm during the nominal event length NUC, (see below). As with PCT-events a  
502 nominal length of MEV-events was defined as the number of hours after the start of an  
503 event by which N25 sank to less than half of N25<sub>av</sub>.

504

505 Three time-related parameters were commonly defined for all three approaches:

506 1. Nominal NPF-event length, (NUC) was nine hours.

507 2. Pre-event periods, (PRENUC), from which increases in diameters or number  
508 concentrations were calculated, were six hours.

509 3. Reference periods, (REF), before PRENUC and after NUC periods were defined in order  
510 to compare event and pre-event data with non-event conditions. Each of these reference  
511 periods had the length of half the sum of pre-event plus event time periods, making the  
512 total reference time period of each event as long as that of the event itself.

513 Besides these common characteristic lengths individual fixed thresholds were chosen and  
514 discussed below for each approach in order to generate at least 200 unique events per  
515 approach, (see Table 2).

516 The aerosol data used to define the NPF-events were complemented by a large number of  
517 environmental parameters. The primary temporal resolution of the environmental parameters  
518 was between one minute (C25, cf. Table 1) and five days (DMSPt, cf. Table 1). C25 was  
519 calculated as 25% percentile on an hourly basis. The parameters with resolutions higher than  
520 an hour (OW, CF, and OC, cf. Table 1) were evaluated along the hourly back trajectories.  
521 While this procedure yielded hourly varying results even of OW, CF, and OC it has to be kept  
522 in mind that this hourly variability is the result of hourly resolved trajectories traversing the  
523 grid; the low primary temporal resolutions of the OW, CF, OC, and chemical parameters  
524 remain. For these slowly varying parameters the REF periods before and after the events  
525 were extended to one day beyond the longest primary resolution, i.e., six days.



526 For two reasons the three search algorithms may yield temporarily redundant results, i.e.,  
527 they may identify the same events. One, they go independently through the same time series  
528 of aerosol data, possibly causing inter-approach redundancy. Two, each algorithm goes  
529 through the time series hour by hour, thus allowing for temporal overlap of events found by  
530 each approach, (intra-approach redundancy).

531 The three types of events were assumed to be mutually exclusive and potentially being  
532 caused by different sets of conditions for new particle formation. Thus, a FORTRAN  
533 procedure was developed to eliminate both intra and inter-approach redundancy while  
534 maintaining a maximum of identified NPF-events. To remove intra-approach redundancy the  
535 procedure identifies overlapping events within each approach. Of each ensemble of such  
536 overlapping events the one with the strongest key parameter of the respective approach  
537 (growth of D50, or concentration increases as defined above) is retained. Next, inter-  
538 approach redundancy is addressed by the procedure. However, there is no unique solution to  
539 the problem of the partly redundant three time series of events. In order to avoid any  
540 preference of one or several types of events in the tests of inter-approach overlap pairs of  
541 events of different approaches are chosen at random and compared for overlap. This random  
542 comparison is done as often as the product of the number of events of the three approaches.  
543 This rather time-consuming random test yields stable numbers of non-overlapping events  
544 within less than one percent, irrespective of the order in which the events of the three  
545 approaches were arranged for the test. By removing intra and inter-approach redundancy in  
546 the first two steps of the procedure a number of time periods will be “freed”. Consequently,  
547 in a last step, the procedure tries to fill the “freed time periods” non-redundantly with events  
548 of the three approaches that had been eliminated in the first two steps. Table 2 collects total  
549 numbers and unique numbers of events for each approach. In the rest of the paper only non-  
550 redundant events will be discussed. The total number of new particle formation events will  
551 be shortened to TNPF.

rev. 2017-2-18 10:48

Gelöscht: -

... [1]

### 554 3.1 The upper percentile of N25 (PCT-approach)

555

556 Events of new particle formation were identified by time periods in which N25 was  
557 consistently, i.e. on average for three hours, above a set threshold. With a threshold of the  
558 93%-percentile ( $170 \text{ cm}^{-3}$ ) 4143 PCT-events were identified in the total data set, only 240 of  
559 which were unique because most of them overlapped with event or pre-event times of the  
560 other two approaches. Average N25 during these unique events was  $330 \text{ cm}^{-3}$  and the average  
561 length of events  $4 \pm 0.9 \text{ h}$ , (one standard deviation).

562 Fig. 4, (top), shows the average temporal development of the relative size distributions for  
563 the unique PCT-events as in the results in Karl et al. (2013), i.e. relative concentrations were  
564 formed by dividing the absolute number concentrations by the average total number during  
565 the six-hour pre-event time periods. The events are characterized by a nearly monomodal  
566 distribution around 20 nm that broadens somewhat around the nominal start of the events.  
567 During the last three hours before the events D50 decreased slightly and returned to the pre-  
568 event level during the nine NUC hours.

569 In connection with PCT-events average aerosol parameters NTO through N300 showed an  
570 average increase by a factor of 2.2 during PRENUC-periods, which was maintained on an  
571 average level of 1.5 during the events. The aerosol-chemical parameters  $\text{Na}^+$ ,  $\text{nssSO}_4^{-2}$ , and  
572 MSA were on an average level of 20% of their reference value. The average environmental  
573 parameters indicate a strong increase by a factor of 14 in solar radiation and a lifting of cloud  
574 base before the events. During the events the level of solar radiation was still elevated by a  
575 factor of six above its reference value. As a consequence temperature at the station was up by  
576 2 – 3 degrees. Precipitation 12 h before trajectory arrival time, (SP12) was a factor of five  
577 above reference levels for air arriving during NUC-periods, whereas SP35 to SP5D were  
578 below their respective reference levels. Cloud fractions were slightly raised 12 - 48 h before  
579 air arrival. Of the ocean parameters more open water was met by trajectories 12 to 24 before

580 their arrival with ocean temperatures 12 to 48 h before trajectory arrival having been up to  
581 four degrees warmer than their respective reference values. On average DMSPt-parameters  
582 OC24 through OC5D showed were raised by a factor of two above their reference value.

583 In Fig. 5, (left top panel), average trajectory height profiles during PRENUC and NUC-  
584 periods are displayed. Widely varying vertical air mass paths occurred before and during  
585 PCT-events. Median vertical trajectory paths during PRENUC and NUC times indicated air  
586 coming from some 300 m above station level five days ago sinking to about one hundred  
587 meters above station level during the last two days before arrival. The upper quartiles of the  
588 PCT-height profiles point at strong subsidence before air mass arrival.

589 The right top panel in Fig. 5 maps average horizontal trajectory positions in 12 h steps in  
590 months having at least ten PCT-events, i.e., May - September. Filled circles around the  
591 trajectory positions comprise 95% of all events. The monthly average horizontal trajectory  
592 direction during PCT-events mostly was from the northwest. In June and July the trajectories  
593 reached farthest into the multiyear ice cover northeast of Greenland. Only during September  
594 the back trajectories covered ice-free and marginal ice areas in the Fram Strait. We note that  
595 the five-day back trajectories of PCT-events, (and of the other two approaches as well), stayed  
596 within some 800 km of Mt. Zeppelin.

597

598

### 599 **3.2 The diameter growth (DGR) approach**

600

601 The DGR-approach to identify events of new particle formation builds on the classical  
602 concept of particle growth through condensable vapors after an initial nucleation of sub-five  
603 nanometer particles that cannot be observed with the available instrumentation, so called  
604 “Banana-type” (Kulmala et al., 2004). The respective algorithm utilizes the parameter D50,  
605 (see Table 1), and requires a growth of this diameter by at least a factor of 1.5 after the

606 nominal start of an event. With this threshold the algorithm searched through all 87646 hours  
607 of the ten-year record and found 1199 DGR-events of new particle formation. After  
608 eliminating cases of temporal overlap with the other two approaches 235 unique events of this  
609 type remained, (see Table 2). Other or more DGR-events could have been found by  
610 shortening the nominal nine NUC hours. For two reasons we refrained from discussing  
611 shorter growth periods in the DGR-approach. Maintaining common-length NUC periods  
612 facilitated the comparison of results of the three approaches. Furthermore, reducing the  
613 growth period would also make PCT and DGR-events ever more similar.

614 In the analysis of atmospheric data and theoretical modeling of NPF-events of type DGR  
615 two key parameters are discussed, namely particle formation rate  $J$  ( $\text{cm}^{-3}\text{s}^{-1}$ ) and growth rate  
616  $GR$  ( $\text{nmh}^{-1}$ ) of particle diameters. For both parameters the measurement protocol by Kulmala  
617 et al. (2012) provides specific calculation procedures, (equations. 2, 7, and 9), which we  
618 follow in the present study, albeit with the caveat that the one-hour temporal resolution of our  
619 time series is far below the ten-minute time resolution that the protocol of Kulmala et al.  
620 (2012) requests in order to be able to follow the rapid development of NPF-events.  
621 Furthermore, only the 127 DGR-events identified from 2011 on are based on particle size  
622 distributions measured down to a diameter of five nanometers.

623 The sizes of newly nucleated aerosol particles are of order 1–2 nm, which is below or near  
624 the limit of existing measurement techniques. When the nuclei grow in size their number  
625 concentration decreases because of various removal mechanisms. Instead of particle  
626 formation rates at the initial nucleus size so-called apparent nucleation rates  $J_x$  are often  
627 reported, i.e. rates at which new particles appear at some larger observable particle diameter  
628  $dx$ . For the present study two apparent nucleation rates are calculated: DGR events of the  
629 whole time series have been identified with particle size distributions measured at diameters  
630 from 10 nm up through the growth of the number median diameter  $D_{50}$  in the size range 10 –  
631 50 nm. Thus we calculated  $J_{22}$  for these 235 events at the nominal geometric mean diameter

rev. 2017-4-7 15:49

Formatiert: Hochgestellt

rev. 2017-4-7 15:50

Formatiert: Hochgestellt

rev. 2017-4-7 15:50

Formatiert: Hochgestellt

632 of 22 nm. For 127 of these events size distributions reached down to five nanometer  
633 diameter, (years 2011 and later). For these events we calculated J11 at the geometric mean  
634 diameter 11 nm as representative for the diameter range 5 – 25 nm, which is close to the  
635 frequently reported apparent formation rate J10 at 10 nm diameter. Additionally, the two  
636 corresponding grow rates GR22 and GR11 were calculated in the respective diameter ranges.

637 Statistics of these four key parameters of the DGR events are collected in Table 3.  
638 Depending on the pollution level at the measuring site widely varying values of J10 have been  
639 reported. For the polluted subtropical environment of Taiwan Young et al. (2013) give values  
640 from 4.4 to 30  $\text{cm}^{-3}\text{s}^{-1}$  whereas Pierce et al. (2014) published values between 0.22 and 0.84  
641  $\text{cm}^{-3}\text{s}^{-1}$  from a rural Canadian setting. The latter range is within the range 0.1 – 9.4  $\text{cm}^{-3}\text{s}^{-1}$   
642 with a median value of 1.2  $\text{cm}^{-3}\text{s}^{-1}$  reported by Yli-Juuti et al. (2009) for a station in rural  
643 Hungary. The two formation rates of the present study cover the range 0.1 – 1.4  $\text{cm}^{-3}\text{s}^{-1}$  for  
644 the 25% to 75% percentiles (see Table 3), which covers the range of 0.05 to 0.13  $\text{cm}^{-3}\text{s}^{-1}$  given  
645 by Vencaz et al. (2009) for a remote site in the Himalaya. The environmental conditions at  
646 the Siberian station Tiksi at the coast of the Laptev Sea may come closest to our Arctic  
647 setting. From this site Asmi et al. (2016) published formation rates of 0.01 to 0.41 at an  
648 unspecified particle size.

649 In terms of 25% to 75% percentiles the particle growth rates of the present study range  
650 from 0.4 to 1.4  $\text{nmh}^{-1}$  in the range 5 – 25 nm and 1.0 to 1.8  $\text{nmh}^{-1}$  in the diameter range 10 -  
651 50 nm, which is near the range of results of 1 – 2  $\text{nmh}^{-1}$  derived by Ström et al. (2009) for  
652 new particle formation in the lower boundary over Ny-Ålesund, Spitsbergen but considerably  
653 lower than the maximum growth rate of 3.6  $\text{nmh}^{-1}$  reported by Asmi et al. (2016) for July at  
654 the Siberian station Tiksi at the coast of the Laptev Sea. For open ocean new particle  
655 formation events over the North Atlantic O'Dowd et al. (2010) report a “typical growth rate”  
656 of 0.8  $\text{nmh}^{-1}$  whereas Ehn et al. (2010) give an average growth rate of 3  $\text{nmh}^{-1}$ . We note that  
657 the average length of DGR-events was  $10 \pm 1$  h, (one standard deviation).

rev. 2017-4-7 18:10

Formatiert: Hochgestellt

rev. 2017-4-7 18:10

Formatiert: Hochgestellt

rev. 2017-4-7 18:42

Gelöscht: Starting with an average value of  $D_{50} \approx 16$  nm at the nominal start of DGR-events an average growth rate of

rev. 2017-4-7 18:43

Gelöscht: 8

rev. 2017-4-7 18:44

Formatiert: Nicht Hochgestellt/ Tiefgestellt

rev. 2017-4-7 18:45

Gelöscht: is derived

rev. 2017-4-7 18:45

Gelöscht: in

rev. 2017-2-18 10:48

Gelöscht: The

665 The average temporal development of the relative number size distribution during DGR-  
666 events is presented in Fig. 4, (center). After a decrease of the sub-50 nm diameter median  
667 from about 25 to 16 nm during the six hours before the nominal start of the events D50  
668 increases systematically during the following nine NUC hours with somewhat reduced growth  
669 towards the end of the event.

670 During the PRENUC-periods particle number concentrations N300, and the condensation  
671 sink, (CS), decreased relative to the reference periods before and after the events.  
672 Subsequently, during the NUC periods the strongest increases was found for N60.  
673 Environmental parameters around air mass arrival showed a strong lifting of cloud base,  
674 (C25), and an extremely high increase in solar radiation, (by a factor of 11 during PRENUC  
675 and by a factor of 60 during NUC periods). However, 12 h before air arrival precipitation had  
676 been up by a factor of 2.5. Cloud fractions were down to about 70% of their reference values  
677 24 through 48 h before air arrival. Of the chemical aerosol parameters  $\text{Na}^+$  and  $\text{nssSO}_4^{-2}$   
678 showed an increase of 2.6 and 2.3, respectively. OC12 and OC48 were slightly higher than  
679 reference level before and during the events. Sea surface temperatures T24 were raised by  
680 nearly one degree whereas earlier SST-values, (T36 – T5D), were up to one degree below  
681 reference values.

682 Fig. 5, (left center panel), shows statistics of the vertical air movement before trajectory  
683 arrival during DGR-events at Mt. Zeppelin covering a wide range of vertical movements  
684 between 200 m and beyond 1500 m height. During the days when elevated DMSPt levels  
685 were noted median trajectory heights were six to nine hundred meters. Median trajectories  
686 during PRENUC times dipped down to the station level, (474 m a.s.l), about one day before  
687 arrival, albeit lifted and subsided again shortly before arrival. Vertical trajectory pathways  
688 will be discussed further in Section 4.2.

689 Monthly average trajectory positions and their variability in connection with DGR-events  
690 are shown in Fig. 5, (center right panel). The months April through October had at least ten

691 DGR-events per month. As with PCT-events the general trajectory direction was from the  
692 northwest, mostly staying for several days over the marginal ice zone between northeastern  
693 Greenland and eastern Svalbard. During the earliest month of April with 14 DGR-events the  
694 back trajectories reached farthest south into the ice-free parts of the Fram Strait.

695

696

### 697 **3.3 The Multiple-size approach (MEV)**

698

699 Leck and Bigg (2010) and Karl et al. (2013; 2012) discussed a type of new particle formation  
700 that to date only has been reported from the summer Arctic. During these MEV-events high  
701 ultrafine particle concentrations appear concurrently in a broad diameter range reaching from  
702 under 10 to some 60 nm. We simulated this type in a search that required the concurrent  
703 increase of NTO, N20, N40, and N60, (cf. Table 1), as averaged over the first three NUC  
704 hours by a factor  $\geq 1.6$  over their respective averages during the six (PRENUC) hours. Over  
705 the ten years of data 1191 such events of this type were identified, 266 of which remained  
706 after removal of those overlapping with events of other approaches. During these unique  
707 events the average concurrent concentration increase was 4.7 and the average length of the  
708 events  $12 \pm 0.8$  h.

709 The concurrent appearance of high concentrations at many particle sizes below 60 nm  
710 resembles the nocturnal NPF-events analyzed by Suni et al. (2008) in the Australian  
711 Eucalyptus forest and simulated in subsequent chamber experiments (Ristovski et al., 2010;  
712 Junninen et al., 2008). We emphasize though that the condensing vapors in the Australian  
713 NPF-events originating from terrestrial biogenic emission are quite different from the  
714 polymer gels implicated in the Arctic MEV-events and originating from the surface  
715 microlayer of the ocean.

716 The bottom part of Fig. 4 shows the average temporal development of relative number size  
717 distributions before and during MEV-events. The development before the nominal start of  
718 MEV-events is more complex than during the PRENUC-periods of the first two types of  
719 events. Intermittently a mode around seven nanometers shows up that broadens and becomes  
720 more prominent about two hours before the nominal start of events. The major PRENUC-  
721 mode around 25 nm also broadens and becomes more prominent towards NUC. A weak  
722 mode exists during PRENUC around 120 nm and hardly any particles beyond 400 nm. D50  
723 sinks from 25 to about 20 nm and stays below 25 nm through the MEV-events even though  
724 number concentrations increase during the first NUC-hours by more than a factor of five.

725 During NUC-periods all particle number concentrations increased, on average by a factor  
726 of 1.6. Average solar radiation also increased by about 90% above reference level during  
727 NUC-periods. Of the chemical parameters  $\text{nssSO}_4^{-2}$  showed an increase by a factor of three  
728 during PRENUC and NUC-periods, and MSA a slight increase during PRENUC-periods. On  
729 one hand, precipitation 12 h, and 36 to 48 h before trajectory arrival, (SP12, SP48), were  
730 above reference levels for air arriving during PRENUC-periods. On the other hand, during  
731 PRE, SP24, SP36, an SP5D indicated dry conditions during PRENUC and NUC-periods.  
732 Only three to five days before air arrival slightly increased cloud fractions were noted. Sea  
733 surface temperatures up to five days before trajectory arrival were on average about one  
734 degree lower than their reference values. DMSPt parameters OC12 to OC36 were raised by  
735 factors of 1.3 and 1.6 during PRENUC and NUC-periods, respectively.

736 Percentiles of vertical trajectory coordinates prior to and during MEV-events are displayed  
737 in Fig. 5, (bottom left panel). During the events, and even stronger during the PRENUC  
738 periods median trajectories had been below 500 m for more than four days. Furthermore, the  
739 final air approach to Mt. Zeppelin mostly came from below the station level. Upper quartiles  
740 of the vertical trajectory positions are substantially lower than with DGR-events. We note,



741 however, that a short excursion above station level occurred in the upper quartiles during the  
742 last three hours before arrival.

743 The bottom right panel of Fig. 5 gives the monthly average trajectory positions and their  
744 variability in connection with MEV-events. The months April through October had at least  
745 ten MEV-events per month. As with the other approaches the general trajectory direction was  
746 from the northwest, albeit with stronger swings towards the ice-free areas south of Svalbard  
747 early and late in the season, (April, May, and September). Interestingly, the trajectories of the  
748 11 MEV-events in October were directed nearly straight north from the North Pole.

749 Summarizing differences and commonalities among the results of the three approaches we  
750 can state that the length of the events increases from four to ten and twelve, going from PCT  
751 to MEV-events. PCT-events are characterized by lower-than-reference aerosol-chemical  
752 parameters.  $\text{Na}^+$  and  $\text{nssSO}_4^{-2}$  show strong increases in the other two types of events:  $\text{Na}^+$  in  
753 connection with DGR-events and  $\text{nssSO}_4^{-2}$  in connection with MEV-events. Both, PCT and  
754 DGR-events exhibit strong increases in solar radiation. Precipitation before air arrival was  
755 raised at varying times in connection with the three types of events. Cloudiness both  
756 increased and decreased at varying times before air arrival with the three types of events.  
757 Increased open water under the trajectories was strongest with DGR-events and least  
758 important with MEV-events. Only in connection with PCT-events strongly raised sea surface  
759 temperature were noted before trajectory arrival. DMSPt related ocean parameters were  
760 raised to varying degrees and at varying times before all NPF-events, most strongly in  
761 connection with PCT-events and least in connection with DGR-events.

762

763

## 764 4. Discussion

765

### 766 4.1. Environmental setting

rev. 2017-2-18 10:48

Gelöscht: bot

rev. 2017-2-18 10:48

Gelöscht:

769

770 The discussion of the results on new particle formation in the Svalbard region builds on the  
771 variability of new particle formation and related environmental parameters on scales of  
772 months, and days. Fig. 1 gives an overview over the geographic areas which were covered by  
773 one, two, and five-day back trajectories to Mt. Zeppelin during the ten years of the present  
774 study covering the months March through October. This figure illustrates that air arriving at  
775 Mt. Zeppelin during the ten summers of the present study came from widely varying regions  
776 from the central ice-covered Arctic via the northern seas and northernmost Scandinavia to  
777 Greenland. One-day back trajectories cover a roundish area from the central east coast of  
778 Greenland via northern Scandinavia to Franz-Josef-Land, North Pole and back to the north  
779 coast of Greenland. Excluding inner Greenland this area is widened by roughly 500 km by 2-  
780 day back trajectories and by at least another 500 km by 5-day back trajectories reaching over  
781 most of Greenland and the adjacent seas west of Greenland. This is a much wider region  
782 from which air may reach Mt. Zeppelin as compared to sites in the inner Arctic as illustrated  
783 in Fig. 2 of Heintzenberg et al. (2015).

784 On the path of trajectories to Mt. Zeppelin quite different ice conditions were met (see,  
785 Fig. 2). On average North Atlantic open waters reached around West Spitsbergen all the way  
786 to Nordaustlandet. Drift ice was passed over by trajectories along the whole east coast of  
787 Greenland. One-day trajectories passed over the marginal ice zone from the Fram Strait to  
788 Franz-Josef Land but also over more contiguous ice close to the North Pole. At times, with  
789 five-day back trajectories, even the marginal ice regions of Baffin Bay and Beaufort Sea were  
790 reached.

791 The long-term geographical distribution of DMSPt in Fig. 3 reflects the water conditions  
792 for phytoplankton biomass around Svalbard. Directly at the coasts of Greenland and Eurasia  
793 increased nutrient availability in coastal and shelf waters (due to continental run-off and  
794 enhanced hydrodynamics) cause localized areas of high DMSPt values. The low DMSPt

795 values further out along the coast of Greenland are due to sea ice reaching through the Fram  
796 Strait far south, (see Fig. 2). A prominent feature in the regional DMS<sub>Pt</sub> distribution is the  
797 tongue of high DMS<sub>Pt</sub>, (intense blue color), and thus high phytoplankton biomass east of this  
798 area, reaching from Spitsbergen to roughly Jan Mayen that lies within one-day back  
799 trajectories. Northward-flowing Atlantic waters, carried by the West Spitsbergen Current,  
800 and southward-flowing fresh surface waters from melting ice, and recirculated Atlantic  
801 waters, carried by the East Greenland Current (Rudels et al., 2005) are meeting. The layering  
802 created by water masses of different density stabilizes the water column and traps  
803 phytoplankton cells at well-lit depths. If sufficient nutrients are available, this can lead to the  
804 development of large phytoplankton blooms, which can result in high concentrations of  
805 DMS<sub>aq</sub>, (see Fig. 2 in Leck and Persson, 1996a).

806 In the ten-year average cloud fractions systematic differences in cloudiness appear.  
807 Depending on transport pathways as identified by the back trajectories, cloudiness varies on  
808 the way to Spitsbergen. The ice-covered areas, (cf. Fig. 2), from the east coast of Greenland  
809 to Franz-Josef-Land exhibit somewhat lower cloud fractions than the ice-free regions  
810 southwest to east of Spitsbergen.

811

812

## 813 **4.2 Seasonal variability**

814

815 Seasonal changes are discussed in terms of monthly averages taken over the ten-year study  
816 period. As expected in Earth's polar regions the seasonal variability of all environmental  
817 parameters is very high as exemplified by the solar flux, (SFL), and the air temperature,  
818 (TEM), at Mt. Zeppelin in Fig. 6. Due to the seasonal change in cloudiness, (cf. Fig. 7), the  
819 seasonal distribution of SFL is not quite symmetrical about midsummer but is skewed slightly  
820 towards the cloud minimum in spring. The air temperature, however, does not peak before

821 July and has a broad shoulder into fall and winter. The first, and partly absolute maxima, of  
822 the seasonal distributions of NPF-events in Fig. 6 coincide with that of the SFL but then drop  
823 of more slowly towards fall than solar radiation. In particular, MEV-events do so and even  
824 have their main maximum in August. The occurrence of all NPF-events drops off sharply in  
825 October. Whereas May as the first month with larger numbers of events is dominated by  
826 PCT-events, followed by DGR and then MEV-events, the contributions of the three NPF-  
827 types are reversed in the last month with high NPF-numbers, i.e., September.

828 Fig. 6 clearly shows that the formation of new particles in the Svalbard region is not  
829 controlled by the late winter-to-early-spring phenomenon of Arctic haze peaking with highest  
830 sulfate-concentrations in March, (cf. Fig. 3 in Heintzenberg, 1989, and Fig. 6), which has a  
831 minimum in the total number of NPF-events. This minimum is in contrast with the maximum  
832 in new particle formation rates found by Croft et al. (2016a) with their global aerosol model.  
833 The high numbers of accumulation mode particles during the Arctic haze months in late  
834 winter and spring yield the annual maximum in condensation sink, (CS in Fig. 6), which  
835 could quench nucleation events and subsequent growth. Thus, even though photochemistry  
836 may produce significant amounts of nucleating material, the freshly formed particles will not  
837 grow to stable size before they are removed via either deposition or coagulation as discussed  
838 by Tunved et al. (2013) and others. An alternative explanation of the late onset of NPF-  
839 events in TNPF in spring lies in the marine biological processes not being activated nearby  
840 during the Arctic haze period yet, (Heintzenberg and Leck, 1994).

841 Fig. 7 collects the seasonal variation of environmental parameters as averaged along the  
842 back trajectories to Mt. Zeppelin. From their minimum in March-April open water conditions  
843 improve until September, after which the pack ice extent under the trajectories rapidly  
844 increases again. The widening open water areas are reflected in sea surface temperatures  
845 under the trajectories that increase until September before they drop off strongly in October.  
846 Consequently, because of its connection to marine biological activity DMSPt increases in the

rev. 2017-2-18 10:48

Gelöscht: (2013) and others.

848 euphotic zone from first photosynthetic light in May until it evens out around July and drops  
849 off in October. Largest DMSPt values are reached in the vicinity of Svalbard, (cf. OC12 in  
850 July and August in Fig. 7), i.e. considerably later than MSA. The ending of DMSPt-curves in  
851 October is due to the lack of data not due to zero-DMSPt. Still, DMSPt concentrations are  
852 expected to be low at this time of the year at temperate to polar latitudes due to low  
853 phytoplankton biomass and low light exposure, (see Fig. 9 in Galí et al., 2015). In terms of  
854 the MODIS-derived cloud fraction cloudiness increases rapidly from its minimum in April  
855 and evens out on a plateau of 80 – 90% after July. The spring-minimum in cloudiness is  
856 confirmed by the maximum in cloud base as indicated by C25 in Fig. 7. This seasonal  
857 distribution of cloudiness does not correspond to the classical picture of near-surface  
858 cloudiness that exhibits near cloud-free conditions in winter and mostly overcast with Arctic  
859 stratus and fogs during the summer months (Warren and Hahn, 2002; Huschke, 1969). We  
860 explain the difference by the specific atmospheric pathways covered by the back trajectories  
861 of the present study (cf. Fig. 1). Trajectory-averaged precipitation parameters (SP12-5D in  
862 Fig. 7) have minima in the period April – May, from which they increase towards their  
863 maxima in fall and winter.

864 The chemical aerosol information derived from the analyses of filters samples has a  
865 relatively low temporal resolution of at least one day combined with frequent gaps of several  
866 days in between samples. Thus, it cannot directly be related to the time periods of NPF-  
867 events. The seasonal distribution of chemical tracers, however, yields important information  
868 about new particle formation. Taken over the whole year  $\text{nssSO}_4^{2-}$  in Fig. 6 is largely  
869 anthropogenic, (Heintzenberg and Leck, 1994), and has its maximum during the peak of  
870 Arctic haze in March and April and its minimum in August, which does not match any  
871 seasonal distribution of NPF-events. We also plotted  $\text{Na}^+$  in Fig. 6 as a tracer of the inorganic  
872 marine aerosol components sea salt.  $\text{Na}^+$  decreases from its winter maximum to its summer  
873 minimum in June/July, again without similarity to the NPF-distributions. Instead, the

874 seasonal distribution of  $\text{Na}^+$  rather closely follows that of the trajectory-derived wind speed  
875 during the last hour before arrival, (not shown in the figure). Wind speed as driver for sea salt  
876 production is a well established phenomenon (Blanchard and Woodcock, 1957). After a steep  
877 rise in April MSA in Fig. 6 sharply peaks in May and then gradually drops off towards its  
878 minimum in October, more gradually than reported for data taken from 1991 to 2004 by  
879 Sharma et al. (2012) and earlier than reported by Heintzenberg and Leck (1994), both at the  
880 same station. Our seasonal distribution of MSA most closely resembles that of SFL, in Fig. 6,  
881 albeit with its peak in May a month earlier than SFL and more strongly skewed towards  
882 spring. According to Leck and Persson (1996b) on average the concentrations of the marine  
883 biogenic sulfur components, (DMS and MSA), fell with a decline rate of about 30% per week  
884 approaching zero values in September explained by reduced ppp (Leck and Persson, (1996a),  
885 (consistent with Becagli et al., 2016).

886 As MSA is the only measured aerosol component with exclusively marine biogenic  
887 sources, we illustrate its seasonal distribution in greater detail in Fig. 8. In this figure MSA-  
888 concentrations measured on Mt. Zeppelin have been extrapolated along 5-day back  
889 trajectories, forming monthly average monthly maps of potential MSA-sources during the  
890 biologically most active months of March through October.

891 Fig. 8 yields several pieces of information that are relevant to the issue of new particle  
892 formation. Early in spring the biological aerosol sources are limited to the North Atlantic and  
893 Norwegian Sea. In April the tongue of newly opened waters between Novaya Zemlya and  
894 Franz-Josef-Land seemingly is beginning to become biologically active. In May this area  
895 widens towards the Barents Sea while the North Atlantic also becomes more active, reaching  
896 the Fram Strait. In August two wide potential source regions cover the region from Northern  
897 Greenland to the northern end of Scandinavia and the region Barents to Kara Sea. In  
898 September even the pack ice north of Svalbard becomes biologically active, (Leck and  
899 Persson, 1996a), and shows potential MSA sources, in particular, north of the northern coast

rev. 2017-2-18 10:48

Gelöscht: items

901 of Greenland. Finally, the very weak potential MSA sources in October appear to be situated  
902 mainly over the Kara Sea and over the North Atlantic.

903 How do these seasonal distributions compare to those of the NPF-events identified by the  
904 three search-approaches defined in Section 3? To address this question we constrained the  
905 average seasonal distribution of environmental parameters to those hours that had been  
906 identified by the NPF-events of the three approaches. However, none of the individual  
907 seasonal distributions of constrained environmental parameters follows closely any of the  
908 NPF-events. In particular, the main MSA peak remains in May, thus one month earlier than  
909 any peak of the NPF-occurrences. To elucidate further potential differences in the three types  
910 of NPF-events we return to the discussion of vertical pathways of related back trajectories,  
911 (see Fig. 5). In this figure all three types of NPF-events exhibit a wide range of vertical  
912 trajectory paths. As we expect the regional sources of primary particles and particle  
913 precursors to be at or near the surface we segregated the NPF-events into subpopulations with  
914 back trajectories that remained a given time below 500 m, (roughly station level). In Fig. 9  
915 we collected the results concerning the 93 NPF-events that occurred with trajectories under  
916 the 500 m limit, i.e., roughly 12% of all events. The top panel shows that the related  
917 trajectories not only stayed below 500 m through most of the last five days before arrival but  
918 close to the surface until they started rising to the station level about 24 h before arrival. The  
919 peak of the sum of event occurrences now coincided with the main MSA peak in May, (see  
920 center panel in Fig. 9). For DGR-events the May-maximum was particularly strong whereas  
921 the PCT-predominantly occurred in May and June and MEV-events remained clustered  
922 around the later part of summer, possibly coupled to SST and DMSPt.

923 A number of environmental parameters indicated substantial deviations from their  
924 respective reference values during the months with most frequent occurrence of this sub-  
925 population of NPF-events. Strongest deviations were noted for precipitation that was elevated  
926 above reference levels two to five days before trajectory arrival, most prominently for DGR-

927 events in May, (by a factor of six 36 h before trajectory arrival). Strong positive deviations in  
928 aerosol-chemical parameters only occurred with Na<sup>+</sup> in PCT and MEV-events, indicating  
929 relatively high wind speeds near sea surface in the related air masses. MSA was elevated up  
930 to 50% above reference levels only during MEV-events. Elevated levels of DMSPt were  
931 noted with all three types of NPF-formation, most prominently for DGR-events 12 to 36  
932 hours before which DMSPt was ~~increased~~ by ~~a factor~~ up to 1.7 relative to reference levels.

933 The bottom panel of Fig. 9 gives average trajectory positions in 12 h steps for the months  
934 May through September. The circles around the steps comprise 95% of all trajectories.  
935 During all months the trajectories stayed in the ice-free and marginal ice zone between Fram  
936 Strait and Eastern Svalbard as illustrated by average July ice cover for the ten study years,  
937 (for average monthly ice covers cf. Fig. 8). In particular during the earliest and latest months  
938 of May and September the trajectories swing farthest south over the open water south of  
939 Svalbard. We note that the complementary sub-population of results with trajectories  
940 remaining above station level did not yield results that differed strongly from those for the  
941 whole population of back trajectories.

942 As a last step in the discussion of seasonal variations in new particle formation a model is  
943 formulated that describes the average sum of NPF-events, (TNPF), as a function of three  
944 parameters, two of which are directly measurable at the site. With the linear combination of  
945 the solar flux, (SFL, Wm<sup>-2</sup>), average sea surface temperature under back trajectories 36 to 48  
946 hours before their arrival at the site, (T48, °C), and condensation sink, (CS, 10<sup>5</sup> s<sup>-1</sup>):

$$TNPF = 0.57 \cdot SFL + 15.4 \cdot T48 - 0.69 \cdot CS$$

947  
948  
949  
950 TNPF as shown in Fig. 10, can be described within an average deviation of 5% taken over the  
951 major months with new particle formation, April - October. Any other of the sea surface  
952 parameters describes TNPF less ~~satisfactorily~~.

rev. 2017-2-18 10:48

Gelöscht:

rev. 2017-2-18 10:48

Gelöscht: raised

rev. 2017-2-18 10:48

Gelöscht: factors

rev. 2017-2-18 10:48

Gelöscht: well



957

958

959

960

### 961 **4.3 Diurnal variability**

962

963 Average hourly occurrence of the three types of NPF-events is plotted in Fig. 11, (top). The  
964 three approaches yield rather similar diel variations. From their minimum during the night  
965 and early morning hours they reach their maximum occurrence between 12 and 16 h UTC in  
966 the afternoon. One might expect the differences between the NPF-types to be due to the  
967 requirement of the three types of NPF formation being mutually exclusive. However, this  
968 constraint does not exclude that they occur at the same time of day, only that they occur at the  
969 same time on the same day.

970 Over the continents new particle formation and growth events of the classical “Banana-  
971 type” usually exhibit an increase in measurable precursors such as sulfuric acid shortly after  
972 sunrise followed by the detection of increased numbers of nanometer-sized particles between  
973 one and two hours later (Kulmala et al., 2004), who deduce a connection to photochemically  
974 produced condensable vapors from this daily pattern. In the Svalbard region the sun is up all  
975 day between mid-April and the end of August. Consequently we would expect the  
976 photochemical production of condensable vapors to have a smaller diurnal amplitude than at  
977 lower latitudes, which in turn should even out the diurnal pattern of NPF-events to some  
978 degree. Despite the relatively small daily variations in solar elevations the solar flux on Mt.  
979 Zeppelin varied on average by more than a factor of five during the sunlit days (see curve  
980 SFL in Fig. 11, bottom). The daily maximum of SFL between 12 and 15 UTC coincides well  
981 with the average diel change in N25 and NPF-occurrence. As expected in particle growth due

982 to condensable vapors after initial nucleation the daily maximum in N10 precedes that of N25  
983 by a few hours.

984 The other process controlling the development of newly formed small particles is the  
985 diurnal development of the planetary boundary layer, (Kulmala et al., 2004). We have no  
986 data on the daily variation in boundary layer structure over or near the measurement site. The  
987 ceilometer data yield the only high-resolution information with some connection to the  
988 structure of the planetary boundary layer. During the summer months these data show a  
989 consistent daily variation with a jump in most frequent hourly cloud base by about 100 m  
990 from about 1570 m after 09 UTC with rather stable values following until 16 UTC, after  
991 which cloud base decreases again to values comparable to the early morning hours. The  
992 hourly medians of the vertical displacement parameter DZ, (see Fig. 11, bottom), provide a  
993 clearer diurnal variation. While being negative throughout the day, i.e. indicating subsiding  
994 air during the last hour before arrival at Mt. Zeppelin, DZ indicates the weakest subsidence in  
995 early afternoon. We interpret diurnal variation in cloud base and DZ as indicative of local  
996 clearing and convection during the day that may be conducive to photochemical processes  
997 and mixing in the boundary layer, both of which would be enhancing new particle formation.

998

999

## 1000 | 5. **Summary and conclusions**

1001

1002 Three different types of events of new particle formation, (NPF), were identified through  
1003 objective search algorithms formulated for the present study. The first and simplest algorithm  
1004 utilizes short-term increases in particle concentrations below 25 nm, (PCT-events). The  
1005 second one builds on the growth of the sub-50 nm diameter-median, (DGR-events), and is  
1006 most closely related to the classical “banana-type” of events, (Kulmala et al., 2004) involving  
1007 the presence of photochemically generated DMS oxidation precursors. The third and most

rev. 2017-2-18 10:48

Gelöscht: Conclusions

1009 complex, so-called multiple-size approach to identifying NPF-events builds on the hypothesis  
1010 of Leck and Bigg (2010), suggesting the concurrent production of polymer gel particles at  
1011 several sizes below about 60 nm, (MEV-events).

1012 In this analysis the possibility that sporadic anthropogenic emissions were interpreted as  
1013 NPF events cannot be excluded completely. However, there are a number of facts arguing  
1014 strongly against this possibility leading to serious misinterpretation of the data:

1015 a) Location and operation of the Mt. Zeppelin station exclude local contamination to a very  
1016 large extent.

1017 b) Manual inspection of the time series by one of the co-authors (PT) further reduced the risk  
1018 of contaminated data.

1019 c) The temporal evolution of MEV events, i.e. concurrent and sustained concentration  
1020 increases at several particle sizes below 60 nm does not correspond to a typical passage of  
1021 stack emissions from a large combustion source, (Ogren and Heintzenberg, 1990). Instead, it  
1022 looks very much like MEV events observed under even stricter constraints on local or  
1023 regional sources of contamination on icebreaker Oden in the central pack ice area, (Karl et al.,  
1024 2013), and also looks similar to nocturnal NPF-events in Australian forests, (Suni et al., 2008;  
1025 Junninen et al., 2008).

1026 With these algorithms NPF-events were identified in a ten-year record of hourly number-  
1027 size distributions taken at the research station on Mt. Zeppelin, Spitsbergen. As a first and  
1028 general conclusion we can state that NPF-events are a summer phenomenon and not related to  
1029 Arctic haze, which is a late winter-to-early spring event. The seasonal distribution of the  
1030 available information on cloudiness does not suggest any direct connection with NPF-  
1031 formation. The MODIS derived cloud fraction generally is very high (70 – 90%) and rather  
1032 evenly distributed over the Svalbard region during the months with high frequencies of NPF-  
1033 events. As already reported in Tunved et al. (2013), NPF-events appear to be somewhat  
1034 sensitive to the available data on precipitation derived from the trajectory model, in particular

rev. 2017-4-3 17:40

Gelöscht: -

rev. 2017-2-18 10:48

Gelöscht: (2013)

1037 when constrained to cases with back trajectories staying below 500 m. In this subpopulation  
1038 of NPF-events DGR-events show the strongest change in precipitation parameters in  
1039 connection with new particle formation.

1040 The seasonal distribution of solar flux suggests some photochemical control that may  
1041 affect marine biological processes generating particle precursors and/or atmospheric  
1042 photochemical processes that generate condensable vapors from precursor gases. Whereas  
1043 the seasonal distribution of the biogenic MSA follows that of the solar flux it peaks before the  
1044 maxima in NPF-occurrence. For PCT-events, and more distinctly so for DGR-events, this  
1045 one-month delay disappears in the subpopulation with back trajectories staying below 500 m.  
1046 MEV-events, however, maintain their peak occurrence later in summer and early fall.

1047 With the limited information on particle size, composition, particle precursors, and  
1048 environmental conditions no definitive statements can be made about the processes leading to  
1049 the formation of new particles in the Svalbard region. A host of findings, however, point to  
1050 varying and rather complex marine biological source processes. The potential source regions  
1051 for all types of new particle formation appear to be restricted to the marginal ice and open  
1052 water areas between Northeastern Greenland and Eastern Svalbard. During earliest and latest  
1053 months with high numbers of NPF-events the back trajectories reach farther south into the  
1054 open waters of the North Atlantic. Depending on conditions yet to be clarified new particle  
1055 formation may become visible as short bursts of particles around 20 nm, (PCT-events), longer  
1056 events involving condensation growth, (DGR-events), or extended events with elevated  
1057 concentrations of particles at several sizes below 100 nm, (MEV-events). The seasonal  
1058 distribution of NPF-events peaks later than that of MSA and, DGR and in particular of MEV-  
1059 events reach into late summer and early fall with much open, warm, and DMSPt-rich waters  
1060 around Svalbard, promoting the production of *Phaeocystis pouchetii* together with polymer  
1061 gels. Consequently, a simple model to describe the seasonal distribution of the total number  
1062 of NPF-events can be based on solar flux, and sea surface temperature, representing

1063 environmental conditions for marine biological activity, and condensation sink, controlling  
1064 the balance between new particle nucleation and their condensational growth. Based on the  
1065 sparse knowledge about the seasonal cycle of gel-forming marine microorganisms and their  
1066 controlling factors we hypothesize that the seasonal distribution of DGR and more so MEV-  
1067 events reflect the seasonal cycle of the gel-forming phytoplankton.

1068 Despite the rather small diel changes expected during the summer Arctic there is a  
1069 significant diurnal variation in aerosol and environmental parameters. Diurnal distributions  
1070 of particle numbers below ten, (N10), and below 25 nm, (N25) follow that of the solar flux  
1071 rather closely with a maximum between 14 and 16 UTC with the maximum of N10 occurring  
1072 a few hours before that of N25. This delay in maxima may be caused by a slow particle  
1073 growth due to photochemically produced condensable vapors. With a peak around noon  
1074 MEV-events show the earliest daily peak occurrence with PCT and DGR-events peaking  
1075 between 15 and 17 h, more closely to the maximum solar flux. Considering the diurnal  
1076 variation in vertical trajectory displacement, (DZ), the early daily maximum in MEV-  
1077 occurrence may be simply controlled by boundary layer dynamics.

1078 With the large database of ten years of aerosol data on Mt. Zeppelin enriched by  
1079 environmental atmospheric and marine data occurrences, pathways and potential source areas  
1080 of different types of new particle formation in the Svalbard region were elucidated by the  
1081 present study. More process related information about new particle formation would require  
1082 dedicated mechanistic experiments with more detailed information on particle precursors,  
1083 ultrafine particles, and boundary layer mixing processes. DGR and MEV-types of new  
1084 particle formation seem to be more closely related to near-surface processes. Thus, a low-  
1085 level site such as the reopened Station Nord, (Nguyen et al., 2016), would be more suitable  
1086 for related mechanistic experiments. Station Nord has the additional advantage of being close  
1087 to the potential source regions of DGR and MEV-events identified by the present study.

1088 | Acknowledgements

rev. 2017-2-18 10:48

Gelöscht: -

... [2]

1091

1092 | The back trajectories created through the local use of the HYSPLIT4 model developed,  
1093 | maintained and generously distributed by the Air Resources Laboratory of NOAA were a

1094 | backbone of the present study. We are very grateful for the ceilometer data provided by the  
1095 | Alfred-Wegener- Institute in Bremerhaven/Potsdam and to NSIDC for their providing daily

1096 | Arctic sea ice data. Complementing our own chemical analyses of Mt. Zeppelin filter data,  
1097 | sodium and sulfate results were taken from the EBAS database at the Norwegian Institute for

1098 | Air Research (<http://ebas.nilu.no>), for which we are indebted to Anne-Gunn Hjellbrekke and  
1099 | Wenche Aas. We thank the NASA Ocean Biology Distributed Active Archive Center

1100 | (OB.DAAC) for access to MODIS datasets. We are indebted to Yafang Cheng and Zhibin  
1101 | Wang for providing the algorithm for calculating the condensation sink. MG acknowledges

1102 | the receipt of a Beatriu de Pinós post-doctoral fellowship funded by the Generalitat de  
1103 | Catalunya. Long-term funding of the DMPS measurements was provided by the Swedish

1104 | Environmental Protection Agency (Naturvårdsverket). We also thank Norwegian Polar  
1105 | Institute for substantial support of the field operation on Mt. Zeppelin.

1106

1107

rev. 2017-2-18 10:48

Gelöscht: HYSPLIT

rev. 2017-2-18 10:48

Gelöscht: most

Literature

- 1110  
 1111  
 1112 Agarwal, J. K., and Sem, G. J.: Continuous flow, single-particle-counting condensation  
 1113 nucleus counter, *J. Aerosol Sci.*, 11, 343-357, 1980.
- 1114 An, N., and Wang, K.: A Comparison of MODIS-Derived Cloud Fraction with Surface  
 1115 Observations at Five SURFRAD Sites, *J. Appl. Meteor. Clim.*, 54, 1009-1020, 2015.
- 1116 Asmi, E., Kondratyev, V., Brus, D., Laurila, T., Lihavainen, H., Backman, J., Vakkari, V.,  
 1117 Aurela, M., Hatakka, J., Viisanen, Y., Uttal, T., Ivakhov, V., and Makshatas, A.:  
 1118 Aerosol size distribution seasonal characteristics measured in Tiksi, Russian Arctic,  
 1119 *Atmos. Chem. Phys.*, 16, 1271-1287, 10.5194/acp-16-1271-2016, 2016.
- 1120 Ayers, G. P., Caine, J. M., Granek, H., and Leck, C.: Dimethylsulfide oxidation and the ratio  
 1121 of methanesulfonate to non sea-salt sulfate in the marine aerosol, *J. Atmos. Chem.*, 25,  
 1122 307-325, 1996.
- 1123 Bates, T. S., Johnson, J. E., Quinn, P. K., Goldan, P. D., Kuster, W. C., Covert, D. C., and  
 1124 Hahn, C. J.: The biogeochemical sulfur cycle in the marine boundary layer over the  
 1125 Northeast Pacific Ocean, *J. Atmos. Chem.*, 10, 59-81, 1990.
- 1126 Becagli, S., Lazzara, L., Marchese, C., Dayan, U., Ascanius, S. E., Cacciani, M., Caiazzo, L.,  
 1127 Di Biagio, C., Di Iorio, T., di Sarra, A., Eriksen, P., Fani, F., Giardi, F., Meloni, D.,  
 1128 Muscari, G., Pace, G., Severi, M., Traversi, R., and Udisti, R.: Relationships linking  
 1129 primary production, sea ice melting, and biogenic aerosol in the Arctic, *Atmos.*  
 1130 *Environ.*, 136, 1-15, <http://dx.doi.org/10.1016/j.atmosenv.2016.04.002>, 2016.
- 1131 Beine, H. J., Argentini, S., Maurizi, A., Mastrantonio, G., and Viola, A.: The local wind field  
 1132 at Ny-Ålesund and the Zeppelin mountain at Svalbard, *Meteorol. Atmos. Phys.*, 78,  
 1133 107-113, 2001.
- 1134 Bélanger, S., Babin, M., and Tremblay, J.-É.: Increasing cloudiness in Arctic damps the  
 1135 increase in phytoplankton primary production due to sea ice receding, *Biogeosciences*,  
 1136 doi:10.5194/bg-5110-4087-2013, 2013.
- 1137 Blanchard, D. C., and Woodcock, A. H.: Bubble formation and modification in the sea and its  
 1138 meteorological significance, *Tellus*, 9, 145-158, 1957.
- 1139 Browse, J., Carslaw, K. S., Mann, G. W., Birch, C. E., Arnold, S. R., and Leck, C.: The  
 1140 complex response of Arctic aerosol to sea-ice retreat, *Atmos. Chem. Phys.*, 14, 7543-  
 1141 7557, 10.5194/acp-14-7543-2014, 2014.
- 1142 Charlson, R. J., Lovelock, J. E., Andreae, M. O., and Warren, S. G.: Oceanic phytoplankton,  
 1143 atmospheric sulphur, cloud albedo and climate, *Nature*, 326, 655-661, 1987.

1144 Croft, B., Martin, R. V., Leaitch, W. R., Tunved, P., Breider, T. J., D'Andrea, S. D., and  
1145 Pierce, J. R.: Processes controlling the annual cycle of Arctic aerosol number and size  
1146 distributions, *Atmos. Chem. Phys.*, 16, 3665-3682, 10.5194/acp-16-3665-2016, 2016a.  
1147 Croft, B., Wentworth, G. R., Martin, R. V., Leaitch, W. R., Murphy, J. G., Murphy, B. N.,  
1148 Kodros, J. K., Abbatt, J. P. D., and Pierce, J. R.: Contribution of Arctic seabird-colony  
1149 ammonia to atmospheric particles and cloud-albedo radiative effect, *Nature*  
1150 *Communications*, 7, 13444, 10.1038/ncomms13444  
1151 <http://www.nature.com/articles/ncomms13444-supplementary-information>, 2016b.  
1152 Dal Maso, M., Kulmala, M., Riipinen, I., Wagner, R., Hussein, T., Aalto, P. P., and Lehtinen,  
1153 K. E. J.: Formation and growth of fresh atmospheric aerosols: eight years of aerosol  
1154 size distribution data from SMEAR II, Hyytiälä, Finland, *Bor. Env. Res.*, 10, 323-336,  
1155 2005.  
1156 Das, R., Granat, L., Leck, C., Praveen, P. S., and Rodhe, H.: Chemical composition of  
1157 rainwater at Maldives Climate Observatory at Hanimaadhoo (MCOH), *Atmos. Chem.*  
1158 *Phys.*, 11, 3743-3755, 10.5194/acp-11-3743-2011, 2011.  
1159 Dee, D. P., Uppala, S. M., Simmons, A. J., Berrisford, P., Poli, P., Kobayashi, S., and  
1160 Bechtold, P.: The ERA - Interim reanalysis: Configuration and performance of the  
1161 data assimilation system, *Q. J. Roy. Meteorol. Soc.*, 137, 553-597, 2011.  
1162 Draxler, R., and Rolph, G.: HYSPLIT (HYbrid Single-Particle Lagrangian Integrated  
1163 Trajectory) Model access via NOAA ARL READY, NOAA Air Resources  
1164 Laboratory, Silver Spring, MD, 2003.  
1165 Ehn, M., Vuollekoski, H., Petäjä, T., Kerminen, V.-M., Vana, M., Aalto, P., de Leeuw, G.,  
1166 Ceburnis, D., Dupuy, R., O'Dowd, C. D., and Kulmala, M.: Growth rates during  
1167 coastal and marine new particle formation in western Ireland, *J. Geophys. Res.*, 115,  
1168 n/a-n/a, 10.1029/2010JD014292, 2010.  
1169 Flyger, H., and Heidam, N. Z.: Ground level measurements of the summer tropospheric  
1170 aerosol in Northern Greenland, *J. Aerosol Sci.*, 9, 157-168, 1978.  
1171 Galí, M., Devred, E., Levasseur, M., Royer, S.-J., and Babin, M.: A remote sensing algorithm  
1172 for planktonic dimethylsulfoniopropionate (DMSP) and an analysis of global patterns,  
1173 *Remote Sens. Environ.*, 171, 171-184, <http://dx.doi.org/10.1016/j.rse.2015.10.012>,  
1174 2015.  
1175 Galí, M., and Simó, R.: A meta - analysis of oceanic DMS and DMSP cycling processes:  
1176 Disentangling the summer paradox, *Global Biochem. Cycles*, 29, 496-515, 2015.



1177 Gao, Q., Leck, C., Rauschenberg, C., and Matrai, P. A.: On the chemical dynamics of  
1178 extracellular polysaccharides in the high Arctic surface microlayer, *Ocean Sci.*  
1179 *Discuss.*, 9, 215–259, 2012.

1180 Heintzenberg, J., Bischof, W., Odh, S.-Å., and Moberg, B.: An investigation of possible sites  
1181 for a background monitoring station in the European Arctic., *International*  
1182 *Meteorological Institute in Stockholm, Department of Meteorology, Stockholm*  
1183 *University, Stockholm, Report Nr. AP-22, 74 pp, 1983.*

1184 Heintzenberg, J., and Larssen, S.: SO<sub>2</sub> and SO<sub>4</sub> in the Arctic: Interpretation of observations at  
1185 three Norwegian Arctic-subArctic stations, *Tellus*, 35B, 255-265, 1983.

1186 Heintzenberg, J.: Arctic haze: air pollution in polar regions, *AMBIO*, 18, 50-55, 1989.

1187 Heintzenberg, J., and Leck, C.: Seasonal variation of the atmospheric aerosol near the top of  
1188 the marine boundary layer over Spitsbergen related to the Arctic sulphur cycle, *Tellus*,  
1189 46B, 52-67, 1994.

1190 Heintzenberg, J., Leck, C., Birmili, W., Wehner, B., Tjernström, M., and Wiedensohler, A.:  
1191 Aerosol number-size distributions during clear and fog periods in the summer high  
1192 Arctic: 1991, 1996, and 2001, *Tellus*, 58B, 41-50, 2006.

1193 Heintzenberg, J., Wehner, B., and Birmili, W.: "How to find bananas in the atmospheric  
1194 aerosol" New approach for analyzing atmospheric nucleation and growth events,  
1195 *Tellus B*, 59, 273-282, 2007.

1196 Heintzenberg, J.: The aerosol-cloud-climate conundrum, *IJGW*, 4, 219-241, 2012.

1197 Heintzenberg, J., Leck, C., and Tunved, P.: Potential source regions and processes of aerosol  
1198 in the summer Arctic, *Atmos. Chem. Phys.*, 15, 6487-6502, [10.5194/acp-15-6487-](https://doi.org/10.5194/acp-15-6487-2015)  
1199 [2015](https://doi.org/10.5194/acp-15-6487-2015), 2015.

1200 Held, A., Brooks, I. M., Leck, C., and Tjernström, M.: On the potential contribution of open  
1201 lead particle emissions to the central Arctic aerosol concentration, *Atmos. Chem.*  
1202 *Phys.*, 11, 3093-3105, [10.5194/acp-11-3093-2011](https://doi.org/10.5194/acp-11-3093-2011), 2011a.

1203 Held, A., Orsini, D. A., Vaattovaara, P., Tjernström, M., and Leck, C.: Near-surface profiles  
1204 of aerosol number concentration and temperature over the Arctic Ocean, *Atmos.*  
1205 *Meas. Tech.*, 4, 1603–1616, 2011b.

1206 Hubanks, P., Platnick, S., King, M., and Ridgway, B.: MODIS Atmosphere L3 Gridded  
1207 Product Algorithm Theoretical Basis, Document (ATBD) and Users Guide, 2015.

1208 Huschke, R. E.: Arctic cloud statistics from "air calibrated" surface weather observations,  
1209 *Rand Corporation Memo. RM 6173-PR, 79 pp, 1969.*

1210 IOCCG: Ocean Colour Remote Sensing in Polar Seas, Report 16, Eds. Babin, M., Arrigo, K.,  
1211 Bélanger, S. and Forget, M.-H., 129 pp, 2015.

1212 Jaenicke, R., and Schütz, L.: Arctic aerosols in surface air, *Idöjaras*, 86, 235-241, 1982.

1213 Junge, C. E.: Air chemistry and Radioactivity, Academic Press, New York and London, 382  
1214 pp., 1963.

1215 Junninen, H., Hulkkonen, M., Riipinen, I., Nieminen, T., Hirsikko, A., Suni, T., Boy, M., Lee,  
1216 S.-H., Vana, M., Tammet, H., Kerminen, V.-M., and Kulmala, M.: Observations on  
1217 nocturnal growth of atmospheric clusters, *Tellus B*, 60, 365-371, 2008.

1218 Karl, M., Gross, A., Leck, C., and Pirjola, L.: Intercomparison of dimethylsulfide oxidation  
1219 mechanisms for the marine boundary layer: Gaseous and particulate sulfur  
1220 constituents, *J. Geophys. Res.*, 112, D15304, 10.1029/2006JD007914, 2007.

1221 Karl, M., Leck, C., Gross, A., and Pirjola, L.: A Study of New Particle Formation in the  
1222 Marine Boundary Layer Over the Central Arctic Ocean using a Flexible  
1223 Multicomponent Aerosol Dynamic Model, *Tellus*, 64B,  
1224 doi:<http://dx.doi.org/10.3402/tellusb.v3464i3400.17158>, 2012.

1225 Karl, M., Leck, C., Coz, E., and Heintzenberg, J.: Marine nanogels as a source of atmospheric  
1226 nanoparticles in the high Arctic, *Geophys. Res. Lett.*, 40, 3738–3743, DOI:  
1227 10.1002/grl.50661, 2013.

1228 Keene, W. C., Pszenny, A. A. P., Galloway, J. N., and Hawley, M. E.: Sea-salt corrections  
1229 and interpretation of constituent ratios in marine precipitation, *J. Geophys. Res.*, 91,  
1230 6647-6658, 1986.

1231 Keller, M. D., Bellows, W. K., and Guillard, R. R. L.: A survey of dimethylsulfide production  
1232 in 12 classes of marine phytoplankton, in: *Biogenic sulfur in the environment*, edited  
1233 by: E.S. Saltzman, and Cooper, W. J., American Chemical Society, Washington, D,  
1234 167–182, 1989.

1235 King, M. D., Platnick, S., Menzel, W. P., Ackerman, S. A., and Hubanks, P. A.: Spatial and  
1236 temporal distribution of clouds observed by MODIS onboard the Terra and Aqua  
1237 satellites, *IEEE Trans. Geosci. Remote Sens.*, 51, 3826–3852, 2013.

1238 Knutson, E. O., and Whitby, K. T.: Accurate Measurement of Aerosol Electrical Mobility  
1239 Moments, *J. Aerosol Sci.*, 6, 453-460, 1975a.

1240 Knutson, E. O., and Whitby, K. T.: Aerosol classification by electric mobility: apparatus,  
1241 theory, and applications, *J. Aerosol Sci.*, 6, 443-451, 1975b.

1242 Kulmala, M., Dal Maso, M., Mäkelä, J. M., Pirjola, L., Väkevä, M., Aalto, P. P.,  
1243 Miikkulainen, P., Hämeri, K., and O'Dowd, C. D.: On the formation, growth and  
1244 composition of nucleation mode particles, *Tellus*, 53B, 479-490, 2001.

1245 Kulmala, M., Vehkamäki, H., Petäjä, T., Dal Maso, M., Lauri, A., Kerminen, V.-M., Birmili,  
1246 W., and McMurry, P. H.: Formation and growth rates of ultrafine atmospheric  
1247 particles: a review of observations, *J. Aerosol Sci.*, 35, 143-176, 2004.

1248 Kulmala, M., Petäjä, T., Nieminen, T., Sipilä, M., Manninen, H. E., Lehtipalo, K., Dal Maso,  
1249 M., Aalto, P. P., Junninen, H., Paasonen, P., Riipinen, I., Lehtinen, K. E. J.,  
1250 Laaksonen, A., and Kerminen, V.-M.: Measurement of the nucleation of atmospheric  
1251 aerosol particles, *Nat. Protocols*, 7, 1651-1667,  
1252 <http://www.nature.com/nprot/journal/v7/n9/abs/nprot.2012.091.html> - [supplementary-](#)  
1253 [information](#), 2012.

1254 Lana, A., Simó, R., Vallina, S. M., and Dachs, J.: Re-examination of global emerging patterns  
1255 of ocean DMS concentration, *Biogeochem.*, 110, 173-182, 2012.

1256 Lannefors, H., Heintzenberg, J., and Hansson, H.-C.: A comprehensive study of physical and  
1257 chemical parameters of the Arctic summer aerosol; results from the Swedish  
1258 expedition Ymer-80, *Tellus*, 35B, 40-54, 1983.

1259 Leck, C., and Persson, C.: The central Arctic Ocean as a source of dimethyl sulfide: Seasonal  
1260 variability in relation to biological activity, *Tellus*, 48B, 156-177, 1996a.

1261 Leck, C., and Persson, C.: Seasonal and short-term variability in dimethyl sulfide, sulfur  
1262 dioxide and biogenic sulfur and sea salt aerosol particles in the arctic marine boundary  
1263 layer, during summer and autumn, *Tellus*, 48B, 272-299, 1996b.

1264 Leck, C., and Bigg, E. K.: Aerosol production over remote marine areas - A new route,  
1265 *Geophys. Res. Lett.*, 23, 3577-3581, 1999.

1266 Leck, C., and Bigg, E. K.: New particle formation of marine biological origin, *Aerosol Sci.*  
1267 *Technol.*, 44, 570-577, 2010.

1268 Leck, C., Gao, Q., Mashayekhy Rad, F., and Nilsson, U.: Size-resolved atmospheric  
1269 particulate polysaccharides in the high summer Arctic, *Atmos. Chem. Phys.*, 13,  
1270 12573-12588, 10.5194/acp-13-12573-2013, 2013.

1271 Lindsay, R., Wensnahan, M., Schweiger, A., and Zhang, J.: Evaluation of seven different  
1272 atmospheric reanalysis products in the Arctic, *J. Clim.*, 27, 2588-2606, 2014.

1273 Liss, P. S., and Merlivat, L.: Air-sea gas exchange rates: Introduction and synthesis, in: *The*  
1274 *Role of Air-Sea Exchange in Geochemical Cycling*, edited by: Buat-Menard, P.,  
1275 Reidel, Norwell, MS, 113-127, 1986.

1276 Maritorea, S., Siegel, D. A., and Peterson, A. R.: Optimization of a semianalytical ocean  
1277 color model for global-scale applications, *Appl. Opt.*, 41.15, 2705-2714, 2002.

1278 Matrai, P. A., and Vernet, M.: Dynamics of the vernal bloom in the marginal ice zone of the  
1279 Barents Sea: Dimethyl sulfide and dimethylsulfoniopropionate budgets, *Journal of*  
1280 *Geophysical Research: Oceans*, 102, 22965-22979, 10.1029/96JC03870, 1997.

1281 Nguyen, Q. T., Glasius, M., Sørensen, L. L., Jensen, B., Skov, H., Birmili, W., Wiedensohler,  
1282 A., Kristensson, A., Nøjgaard, J. K., and Massling, A.: Seasonal variation of  
1283 atmospheric particle number concentrations, new particle formation and atmospheric  
1284 oxidation capacity at the high Arctic site Villum Research Station, Station Nord,  
1285 *Atmos. Chem. Phys.*, 16, 11319–11336, 10.5194/acp-2016-205, 2016.

1286 Norman, A. L., Barrie, L. A., Toom-Sauntry, D., Sirois, A., Krouse, H. R., Li, S. M., and  
1287 Sharma, S.: Sources of aerosol sulphate at Alert: Apportionment using stable isotopes,  
1288 *J. Geophys. Res.*, 104, 11619-11631, 1999.

1289 O'Dowd, C., Monahan, C., and Dall'Osto, M.: On the occurrence of open ocean particle  
1290 production and growth events, *Geophys. Res. Lett.*, 37, L19805,  
1291 doi:19810.11029/12010GL044679, 2010.

1292 Ogren, J. A., and Heintzenberg, J.: Parametric aerosol sampling at low concentration levels,  
1293 Department of Meteorology, Stockholm UniversityAA-1, 1990.

1294 Orellana, M. V., Matrai, P. A., Janer, M., and Rauschenberg, C. D.:  
1295 Dimethylsulfoniopropionate storage in *Phaecystis* (Prymnesiophyceae) secretory  
1296 vesicles *J. Phycol.*, 47, 112-117, 10.1111/j.1529-8817.2010.00936.x, 2011a.

1297 Orellana, M. V., Matrai, P. A., Leck, C., Rauschenberg, C. D., Lee, A. M., and Coz, E.:  
1298 Marine microgels as a source of cloud condensation nuclei in the high Arctic, *PNAS*,  
1299 108, 13612–13617, 2011b.

1300 Pierce, J. R., Westervelt, D. M., Atwood, S. A., Barnes, E. A., and Leitch, W. R.: New-  
1301 particle formation, growth and climate-relevant particle production in Egbert, Canada:  
1302 analysis from 1 year of size-distribution observations, *Atmos. Chem. Phys.*, 14, 8647-  
1303 8663, 10.5194/acp-14-8647-2014, 2014.

1304 Pirjola, L., Kulmala, M., Wilck, M., Bischoff, A., Stratmann, F., and Otto, E.: Formation of  
1305 sulphuric acid aerosols and cloud condensation nuclei: An expression for significant  
1306 nucleation and model comparison, *J. Aerosol Sci.*, 30, 1079-1094, 1999.

1307 Polissar, A. V., Hopke, P. K., Paatero, P., Kaufman, Y. J., Hall, D. K., Bodhaine, B. A.,  
1308 Dutton, E. G., and Harris, J. M.: The aerosol at Barrow, Alaska: long-term trends and  
1309 source locations, *Atmos. Environ.*, 33, 2441-2458, 1999.

1310 Rahn, K. A., and Shaw, G. E.: Particulate air pollution in the Arctic: Large-scale occurrence  
1311 and meteorological controls, in: Atmospheric Aerosols and Nuclei, edited by: Roddy,  
1312 F., and O'Connor, T. C., Dept. of Physics, University College, Galway, Ireland 21-27  
1313 Sept., 223-227, 1977.

1314 Ristovski, Z. D., Suni, T., Kulmala, M., Boy, M., Meyer, N. K., Duplissy, J., Turnipseed, A.,  
1315 Morawska, L., and Baltensperger, U.: The role of sulphates and organic vapours in  
1316 growth of newly formed particles in a eucalypt forest, *Atmos. Chem. Phys.*, 10, 2919-  
1317 2926, 10.5194/acp-10-2919-2010, 2010.

1318 Rudels, B., Björk, G., Nilsson, J., Winsor, P., Lake, I., and Nohr, C.: The interaction between  
1319 waters from the Arctic Ocean and the Nordic Seas north of Fram Strait and along the  
1320 East Greenland Current: results from the Arctic Ocean-02 Oden expedition, *Journal of*  
1321 *Marine Systems*, 55, 1-30, 2005.

1322 Schmidtko, S., Johnson, G. C., and Lyman, J. M.: MIMOC: A global monthly isopycnal  
1323 upper-ocean climatology with mixed layers, *Journal of Geophysical Research:*  
1324 *Oceans*, 118, 1658-1672, 10.1002/jgrc.20122, 2013.

1325 Schoemann, V., Becquevort, S., Stefels, J., Rousseau, V., and Lancelot, C.: Phaeocystis  
1326 blooms in the global ocean and their controlling mechanisms: a review, *Journal of Sea*  
1327 *Research*, 53, 43-66, <http://dx.doi.org/10.1016/j.seares.2004.01.008>, 2005.

1328 Sharma, S., Chan, E., Ishizawa, M., Toom-Sauntry, D., Gong, S. L., Li, S. M., Tarasick, D.  
1329 W., Leaitch, W. R., Norman, A., Quinn, P. K., Bates, T. S., Levasseur, M., Barrie, L.  
1330 A., and Maenhaut, W.: Influence of transport and ocean ice extent on biogenic aerosol  
1331 sulfur in the Arctic atmosphere, *J. Geophys. Res.*, 117, D12209,  
1332 10.1029/2011JD017074, 2012.

1333 Simó, R.: Production of atmospheric sulfur by oceanic plankton: biogeochemical, ecological  
1334 and evolutionary links, *Trends in Ecology & Evolution*, 16, 287-294, 2001.

1335 Stohl, A.: Computations, accuracy and applications of trajectories - A review and  
1336 bibliography, *Atmos. Environ.*, 32, 947-966, 1998.

1337 Ström, J., Engvall, A.-C., Delbart, F., Krejci, R., and Treffeisen, R.: On small particles in the  
1338 Arctic summer boundary layer: observations at two different heights near Ny-Ålesund,  
1339 Svalbard, *Tellus B - Chemical and Physical Meteorology*, 61, 473-482, 2009.

1340 Suni, T., Kulmala, M., Hirsikko, A., Bergman, T., Laakso, L., Aalto, P. P., Leuning, R.,  
1341 Cleugh, H., Zegelin, S., Hughes, D., van Gorsel, E., Kitchen, M., Vana, M., Hörrak,  
1342 U., Mirme, S., Mirme, A., Sevanto, S., Twining, J., and Tadros, C.: Formation and

1343 characteristics of ions and charged aerosol particles in a native Australian Eucalypt  
1344 forest, *Atmos. Chem. Phys.*, 8, 129-139, 10.5194/acp-8-129-2008, 2008.

1345 Tunved, P., Ström, J., and Krejci, R.: Arctic aerosol life cycle: linking aerosol size  
1346 distributions observed between 2000 and 2010 with air mass transport and  
1347 precipitation at Zeppelin station, Ny-Ålesund, Svalbard, *Atmos. Chem. Phys.*, 13,  
1348 3643–3660, 10.5194/acpd-12-29967-2012, 2013.

1349 Venzac, H., Sellegri, K., Villani, P., Picard, D., and Laj, P.: Seasonal variation of aerosol size  
1350 distributions in the free troposphere and residual layer at the Puy de Dôme station,  
1351 France, *Atmos. Chem. Phys.*, 9, 1465-1478, 10.5194/acp-9-1465-2009, 2009.

1352 Warren, S. G., and Hahn, C. J.: Cloud climatology, in: *Encyclopedia of Atmospheric*  
1353 *Sciences*, edited by: Holton, J. R., Pyle, J., and Curry, J. A., Academic Press, London,  
1354 UK, 476-483, 2002.

1355 Wiedensohler, A., Covert, D., Swietlicki, E., Aalto, P., Heintzenberg, J., and Leck, C.:  
1356 Occurrence of an ultrafine particle mode less than 20 nm in diameter in the marine  
1357 boundary layer of the Arctic summer and autumn, *Tellus*, 48B, 213-222, 1996.

1358 Willis, M. D., Burkart, J., Thomas, J. L., Köllner, F., Schneider, J., Bozem, H., Hoor, P. M.,  
1359 Aliabadi, A. A., Schulz, H., Herber, A. B., Leaitch, W. R., and Abbatt, J. P. D.:  
1360 Growth of nucleation mode particles in the summertime Arctic: a case study, *Atmos.*  
1361 *Chem. Phys. Discuss.*, 2016, 1-31, 10.5194/acp-2016-256, 2016.

1362 Yli-Juuti, T., Riipinen, I., Pasi, A., Nieminen, T., Maenhaut, W., Janssens, A., Claeys, M.,  
1363 Salma, I., Ocskay, R., Hoffer, A., Imre, K., and Kulmala, M.: Characteristics of new  
1364 particle formation events and cluster ions at K-pusztá, Hungary, *Boreal Environment*  
1365 *Research*, 14, 2009.

1366 Young, L. H., Lee, S. H., Kanawade, V. P., Hsiao, T. C., Lee, Y. L., Hwang, B. F., Liou, Y.  
1367 J., Hsu, H. T., and Tsai, P. J.: New particle growth and shrinkage observed in  
1368 subtropical environments, *Atmos. Chem. Phys.*, 13, 547-564, 10.5194/acp-13-547-  
1369 2013, 2013.

1370 Zhang, M., Chen, L., Xu, G., Lin, Q., and Liang, M.: Linking Phytoplankton Activity in  
1371 Polynyas and Sulfur Aerosols over Zhongshan Station, East Antarctica, *J. Atmos. Sci.*,  
1372 72, 4629-4642, 2015.

1373  
1374  
1375

| Parameter                        | TR (h)       | Explanation                                                                                                   |
|----------------------------------|--------------|---------------------------------------------------------------------------------------------------------------|
| C25                              | 1 min        | 25% percentile of cloud base from AWI ceilometer (m)                                                          |
| CF12, 24, 36, 48, 5D             | 24           | Average MODIS cloud fraction during the last 12h, 24h, 36, 48h, and days 3-5 before trajectory arrival        |
| D50                              | 1            | Number-median diameter of particles < 50 nm diameter                                                          |
| CS                               | 1            | Condensation sink ( $s^{-1}$ )                                                                                |
| DZ                               | 1            | Vertical trajectory displacement ( $m h^{-1}$ ) during the last hour before arrival                           |
| MSA                              | $\geq 1$ day | Methane sulfonate ( $nmol m^{-3}$ )                                                                           |
| N10                              | 1            | Number concentration of particles up to 10 nm ( $>2010, cm^{-3}$ )                                            |
| N20                              | 1            | Number concentration between 10 and 20 nm ( $cm^{-3}$ )                                                       |
| N25                              | 1            | Number concentration of particles up to 25 nm ( $cm^{-3}$ )                                                   |
| N40                              | 1            | Number concentration between 20 and 40 nm ( $cm^{-3}$ )                                                       |
| N60                              | 1            | Number concentration between 40 and 60 nm ( $cm^{-3}$ )                                                       |
| N100                             | 1            | Number concentration between 60 and 100 nm ( $cm^{-3}$ )                                                      |
| N300                             | 1            | Number concentration between 100 and 300 nm ( $cm^{-3}$ )                                                     |
| Na                               | $\geq 1$ day | Sodium concentrations ( $nmol m^{-3}$ )                                                                       |
| NCO                              | 1            | Number concentration of particles > 300 nm ( $cm^{-3}$ )                                                      |
| nssSO <sub>4</sub> <sup>2-</sup> | $\geq 1$ day | Non-sea salt sulfate concentrations ( $nmol m^{-3}$ )                                                         |
| NTO                              | 1            | Number concentration of particles $\geq 10$ nm, ( $cm^{-3}$ )                                                 |
| OC12, 24, 36, 48, 5D             | 120          | Average MODIS DMSPt (nmol) during the last 12h, 24h, 36, 48h, and days 3-5 before trajectory arrival          |
| OW12, 24, 36, 48, 5D             | 24           | Average open water (%) during the last 12h, 24h, 36, 48h, and days 3-5 before trajectory arrival              |
| PRE                              | 1            | Trajectory precipitation (mm) at arrival                                                                      |
| RH                               | 1            | Trajectory relative humidity (%) at arrival                                                                   |
| SFL                              | 1            | Solar flux at trajectory arrival ( $W m^{-2}$ )                                                               |
| SP12, 24, 36, 48, 5D             | 1            | Accumulated precipitation (mm) during the last 12h, 24h, 36, 48h, and days 3-5 before trajectory arrival      |
| T12, 24, 36, 48, 5D              | 24           | Average sea surface temperature (C) during the last 12h, 24h, 36, 48h, and days 3-5 before trajectory arrival |
| TEM                              | 1            | Trajectory temperature (C) at arrival                                                                         |
| WDR                              | 1            | Trajectory wind direction ( $^{\circ}$ ) during the last hour before arrival                                  |
| WSP                              | 1            | Trajectory wind speed ( $m sec^{-1}$ ) during the last hour before arrival                                    |

1377

1378

Table 1 Aerosol, atmospheric, and ocean parameters utilized in the present study.

1379

DMSPt = Total dimethylsulfoniopropionate in surface ocean waters. TR = temporal

1380

resolution in which the respective data were available. [All parameter explanations](#)

1381

[starting with "Trajectory" refer to parameters calculated by HYSPLIT4 at each](#)

1382

[trajectory step.](#)

1383

1384  
 1385  
 1386  
 1387  
 1388  
 1389  
 1390  
 1391

| Approach          | Acronym | Criteria and thresholds | Total number of events | Number of unique events | <u>% of total number of data hours</u> |
|-------------------|---------|-------------------------|------------------------|-------------------------|----------------------------------------|
| Percentiles       | PCT     | N25 >93%-percentile     | 4143                   | 240                     | <u>1</u>                               |
| Diameter-growth   | DGR     | D50-Growth >1.5         | 1199                   | 235                     | <u>3</u>                               |
| Multi-size growth | MEV     | Multi-growth >1.6       | 1191                   | 266                     | <u>4</u>                               |
| Sum               |         |                         | 6533                   | 741                     |                                        |

rev. 2017-2-18 10:48  
 Formatierte Tabelle  
 rev. 2017-2-18 10:48  
 Eingefügte Zellen

1392  
 1393  
 1394  
 1395  
 1396

Table 2 Total and unique number of events of new particle formation identified by the three approaches to identify NPF-events, and percent of all data hours covered by unique events.



1397

| <u>Statistics</u> | <u>J11</u> | <u>GR11</u> | <u>J22</u> | <u>GR22</u> |
|-------------------|------------|-------------|------------|-------------|
| <u>Minimum</u>    | <u>0.1</u> | <u>-1.2</u> | <u>0.1</u> | <u>-0.1</u> |
| <u>25%</u>        | <u>0.4</u> | <u>0.1</u>  | <u>0.2</u> | <u>1.0</u>  |
| <u>50%</u>        | <u>0.7</u> | <u>0.4</u>  | <u>0.3</u> | <u>1.4</u>  |
| <u>75%</u>        | <u>1.4</u> | <u>0.6</u>  | <u>0.7</u> | <u>1.8</u>  |
| <u>Maximum</u>    | <u>19</u>  | <u>2.2</u>  | <u>22</u>  | <u>4</u>    |

rev. 2017-4-7 17:47  
**Formatiert:** Schriftart:Fett

rev. 2017-4-7 17:48  
**Formatierte Tabelle**

1398

1399

1400

1401

1402

1403

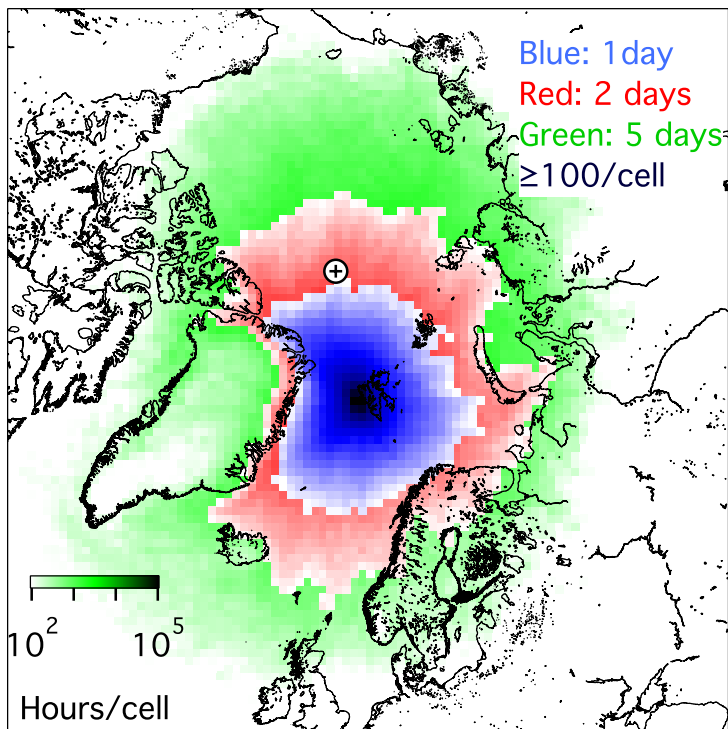
Table 3 Statistics of particle formation rates of DGR-events J11, and J22, ( $\text{cm}^{-3}\text{s}^{-1}$ ), at the nominal geometric mean diameters 11 nm, and 22 nm and corresponding diameter growth rates GR11, and GR22, ( $\text{nmh}^{-1}$ ) in the two diameter ranges 5 – 25 nm, and 10 – 50 nm.

rev. 2017-4-7 17:48  
**Formatiert:** Hochgestellt

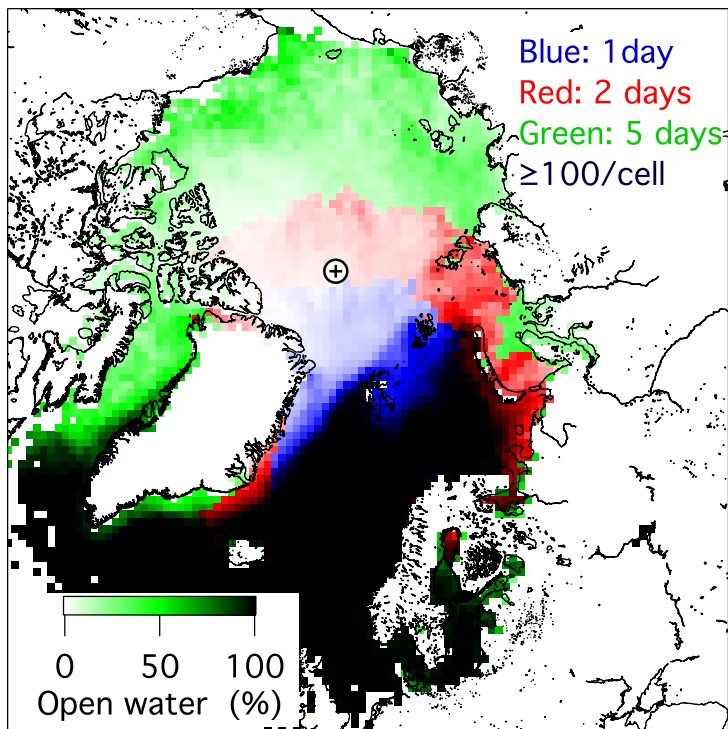
rev. 2017-4-7 17:48  
**Formatiert:** Hochgestellt

rev. 2017-4-7 17:48  
**Formatiert:** Hochgestellt

rev. 2017-2-18 10:48  
**Gelöscht:** .



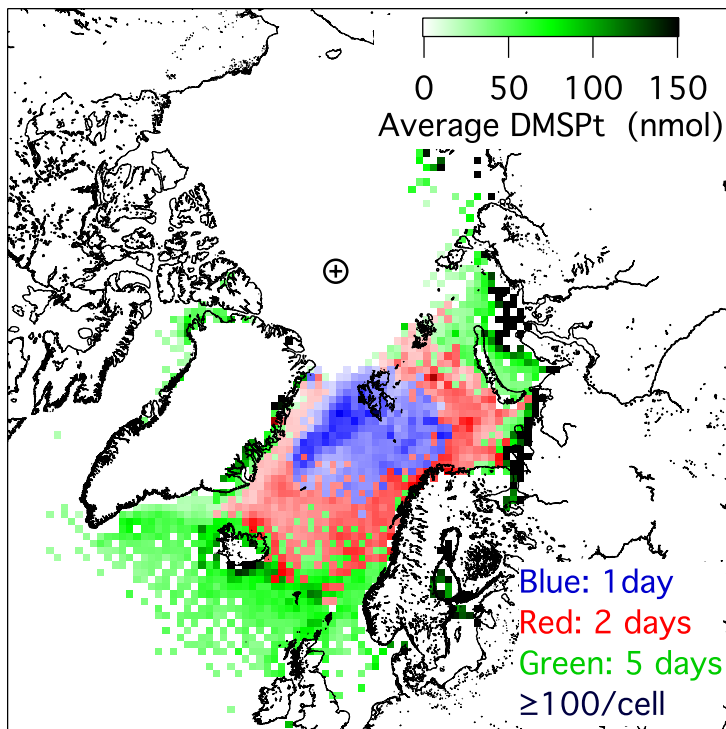
1405  
 1406 Fig. 1 Map of the regional distribution of 5-day (green), 2-day (red), and 1-day (blue)  
 1407 hourly back trajectories to Mt. Zeppelin during the months March through October  
 1408 of the years 2006 - 2015. Black symbol: North Pole. The colored areas are covered  
 1409 with at least 100 trajectory hours per geocell and the color saturation corresponds to  
 1410 the number of trajectory hours per grid cell on a log-scale.  
 1411



1412

1413 Fig. 2 Map of the regional distribution of open water under 87648 5-day (green), 2-day  
 1414 (red), and 1-day (blue) hourly back trajectories to Mt. Zeppelin during the during the  
 1415 months March through October of the years 2006-2015. Black symbol: North Pole.  
 1416 The areas are covered with at least 100 trajectory hours concurrent with data values  
 1417 per geocell.

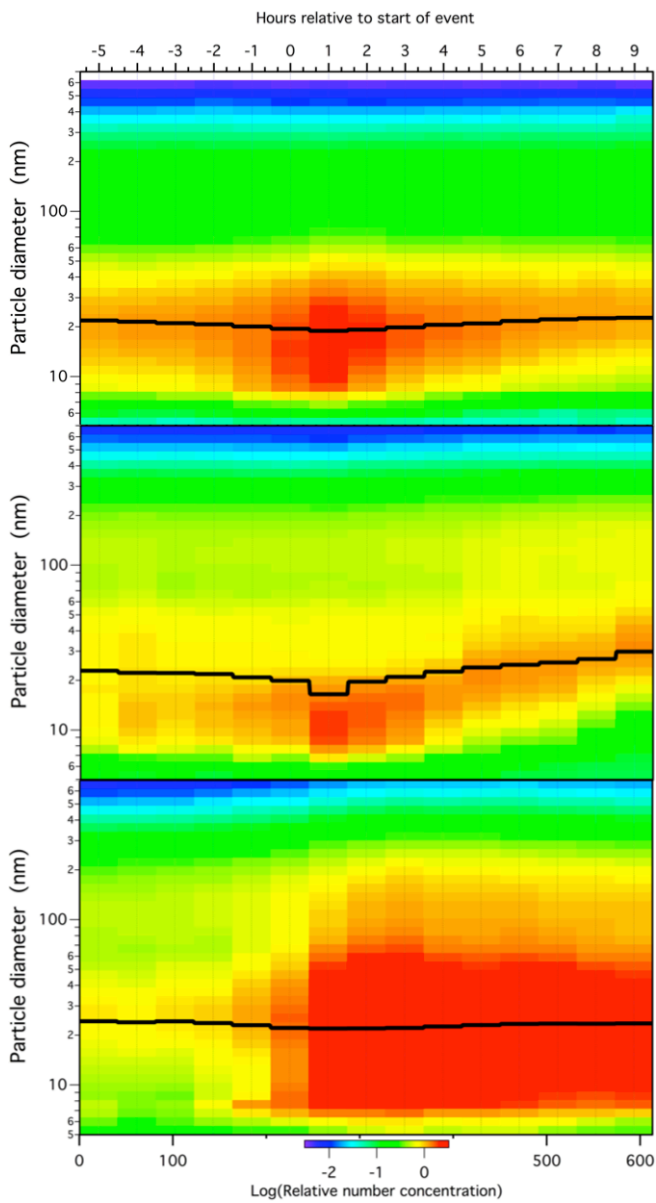
1418



1419

1420 Fig. 3 Map of the regional distribution of DMSPt along 87648 5-day (green), 2-day (red),  
 1421 and 1-day (blue) hourly back trajectories to Mt. Zeppelin during the during the  
 1422 months March through October of the years 2006-2015. Black symbol: North Pole.  
 1423 The relative color scale holds for all colors. The areas are covered with at least 100  
 1424 trajectory hours with data values per geocell.

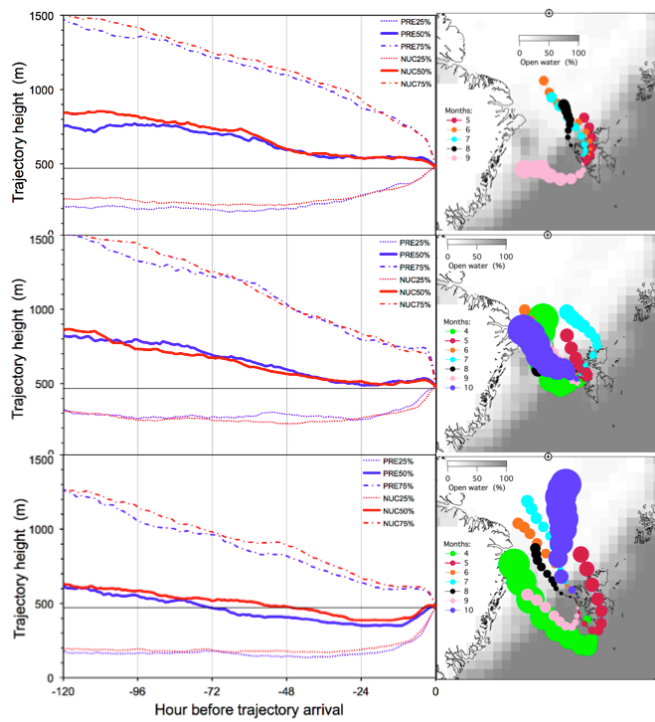
1425



1426

1427 Fig.4 Average temporal development of the relative number size distribution before and  
 1428 during NPF-events identified by the three approaches. The black curve gives the  
 1429 median sub-50-nm particle diameter D50 during the events. Top: PCT-events;  
 1430 center: DGR-events; bottom: MEV-events.

1431

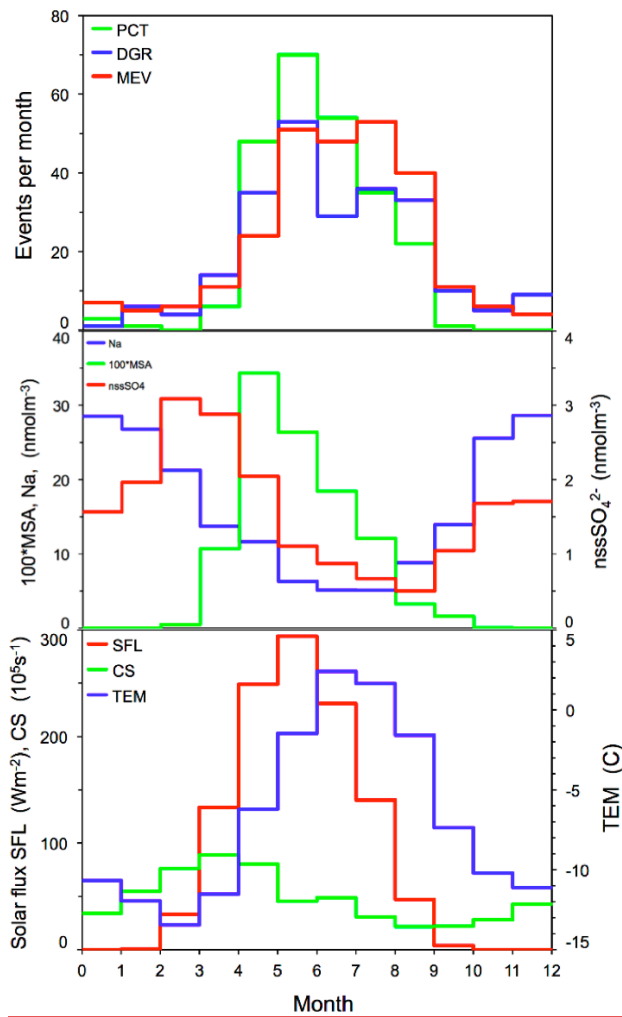


1432

1433 Fig. 5 Left panels: Median back trajectory height profiles (m) during the six pre-event  
 1434 hours (full line in blue, PRENUC) and during the nine DGR-event hours (full line in  
 1435 red, NUC). 25% and 75% percentiles are shown as dotted, and dash-dotted lines,  
 1436 respectively. Top: PCT-events; center: DGR-events; bottom: MEV-events. The thin  
 1437 horizontal line marks the station level.

1438 Right panels: Average monthly trajectory positions in 12 h steps for the months April  
 1439 through October. Only months with at least 10 NPF-events are shown. The circles  
 1440 comprise 95% of all trajectories at any trajectory step. The underlying grey-scale  
 1441 map indicates July ice cover averaged over the years 2006 – 2015

1442



1443

1444 Fig. 6 Top: Monthly numbers of new particle formation events according to the three

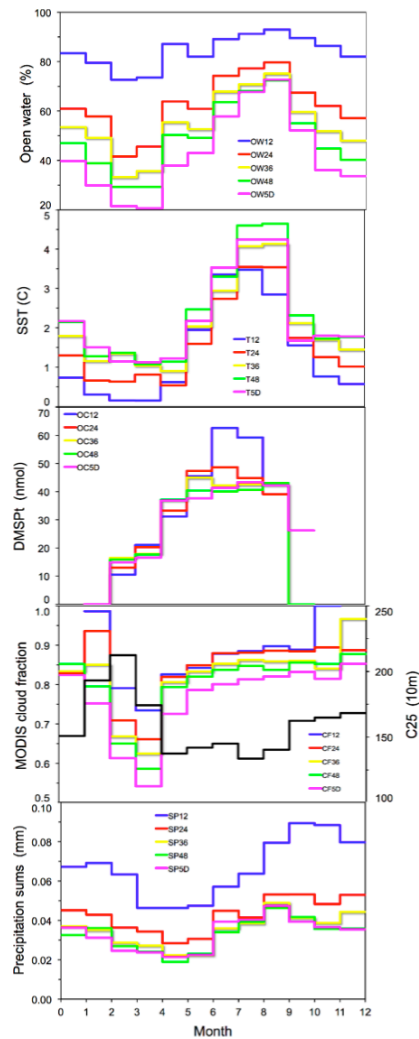
1445 approaches, summed up over the whole period of ten years, PCT: Upper percentile  
 1446 of N25; DGR: Diameter growth; MEV: Multiple size events.

1447 Center: Average seasonal distribution of particle composition in  $\text{nmolm}^{-3}$ .  
 1448 Na = sodium,  $\text{nssSO}_4^{2-}$  =  $\text{nssSO}_4^{2-}$ , MSA = Methane sulfonate times 100.

1449 Bottom: Monthly average solar flux (SFL, red,  $\text{Wm}^{-2}$ ), and temperature (TEM, blue  
 1450  $^{\circ}\text{C}$ ), and condensation sink, (CS,  $10^5\text{s}^{-1}$ ), at Mt. Zeppelin, Spitsbergen.

1451

rev. 2017-2-18 10:48  
 Gelöscht: .

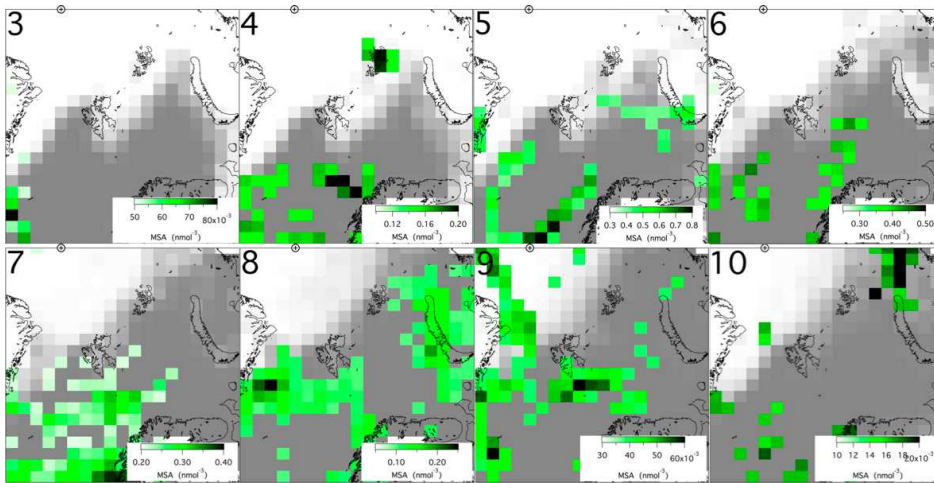


1454

1455 Fig. 7 Monthly averages of environmental parameters averaged along back trajectories to  
 1456 Mt. Zeppelin. From top to bottom: OW12-5D: Open water in % during last 12, 24,  
 1457 36, and 48h, and days 3-5 before trajectory arrival at Mt. Zeppelin. T12-5D: Same  
 1458 for sea surface temperature in °C. OC12-5D: Same for DMSPt in nmol in surface  
 1459 waters. CF12-5D: Same for MODIS cloud fraction. SP12-5D: Same for  
 1460 precipitation sums in mm. C25 = 25%-percentile of cloud base in decameter.

1461





1462

1463

1464

1465

1466

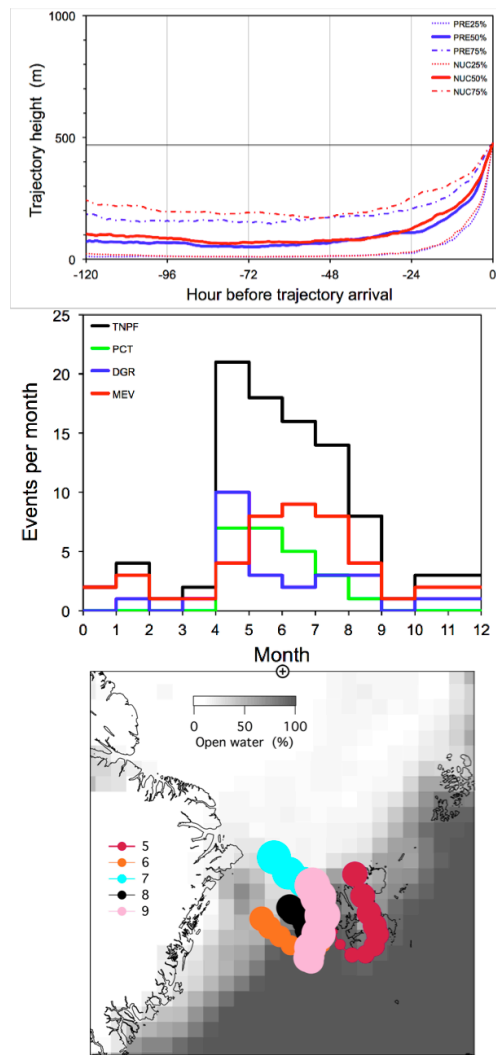
1467

1468

1469

1470

Fig. 8 Average monthly distribution of methane sulfonic acid, (MSA,  $\text{nmolm}^{-3}$ ), during the months March–October of the years 2006–2015, constructed from MSA-concentrations measured on Mt. Zeppelin, which were extrapolated along 5-day back trajectories. Average open water percentages during the respective months are indicated as white (0% open water) to dark grey (100% open water) areas. The position of the North Pole is marked as cross in circle on the upper border of the maps.



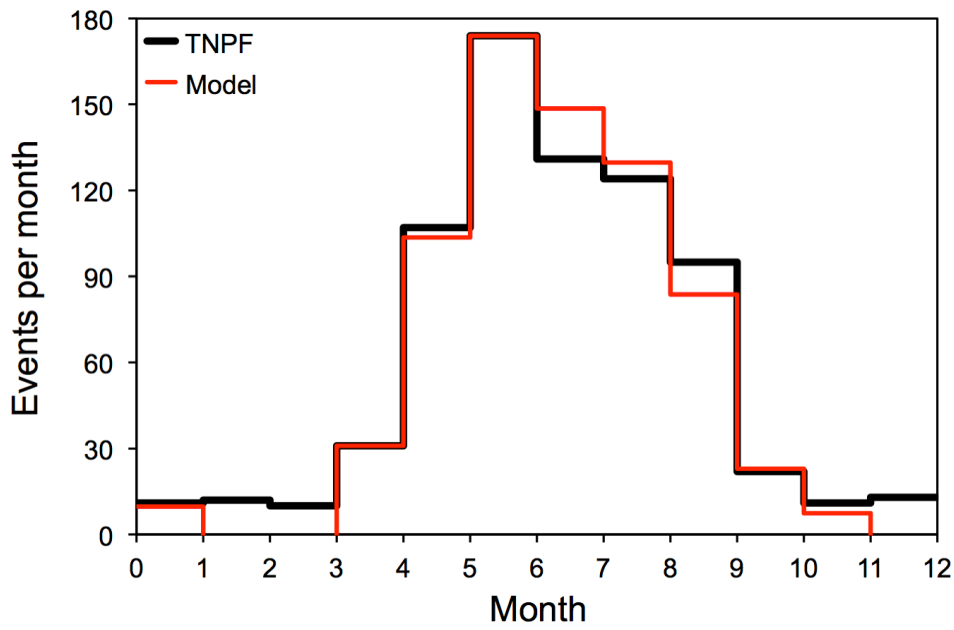
1471

1472 Fig. 9 Characteristics of the subpopulation of 93 NPF-events with back trajectories that  
 1473 stayed below 500 m for five days before arrival. Top: Statistics of related vertical  
 1474 trajectory coordinates as in Fig. 5. Center: Average monthly occurrence of PCT,  
 1475 DGR, and MEV-events, summed up over the whole period of ten years. Bottom:  
 1476 Related average monthly trajectory positions in 12 h steps for the months May  
 1477 through September. The circles comprise 95% of all trajectories at any trajectory

rev. 2017-2-18 10:48

Gelöscht: .

1479 step. The underlying grey-scale map indicates July ice cover averaged over 2006 –  
1480 2015.  
1481

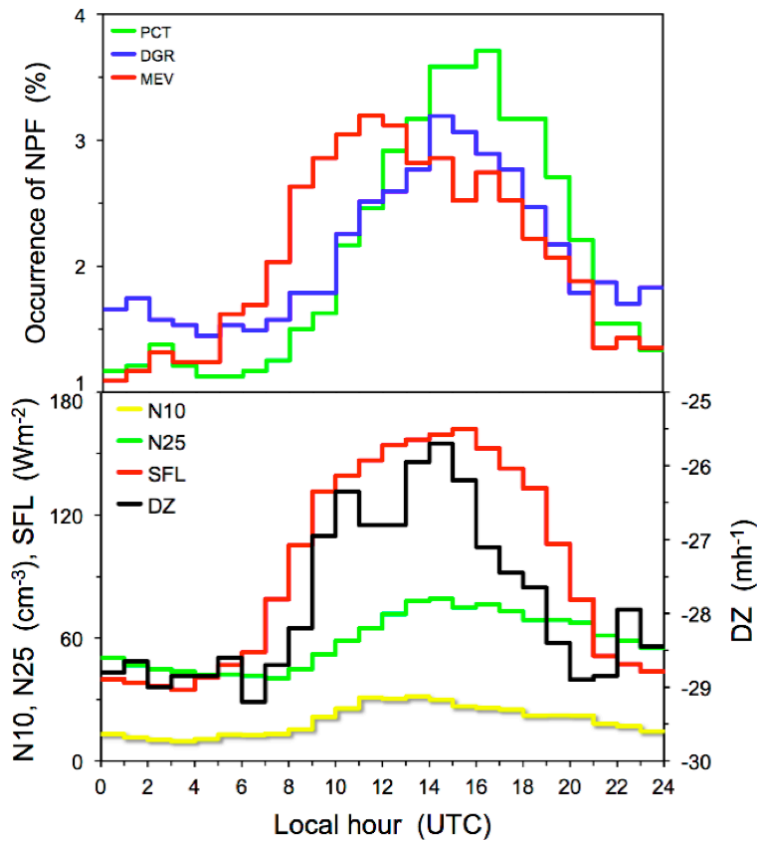


1482

1483 Fig. 10 Average monthly sums of NPF-events due to the three types of new particle  
 1484 formation, (TNPF, black), summed up over the whole period of ten years, Red:  
 1485 Three-parameter model to describe TNPF.

1486

rev. 2017-2-18 10:48  
 Gelöscht: )



1488

1489 Fig. 11 Top: Relative average diurnal occurrence of the three types NPF-events. PCT:  
 1490 Upper percentile of N25; DGR: Diameter growth; MEV: Multiple size events.  
 1491 Bottom: Average diurnal variation of the HYSPLIT-modeled solar flux (SFL, Wm<sup>-2</sup>),  
 1492 the integral particle concentrations N10, and N25 in cm<sup>-3</sup>, and of the vertical  
 1493 displacement parameter (DZ, mh<sup>-1</sup>). N10 is based on data of the years 2011 – 2015  
 1494 whereas the other parameters are based on data of the years 2006 – 2015.